2015-01-01

An Improved Sin-Hyperbolic Constitutive Model For Creep Deformation And Damage

Mohammad Shafinul Haque
University of Texas at El Paso, mhaque@miners.utep.edu

AN IMPROVED SIN-HYPERBOLIC CONSTITUTIVE MODEL FOR CREEP DEFORMATION AND DAMAGE

MOHAMMAD SHAFINUL HAQUE

Department of Mechanical Engineering

APPROVED:

Calvin M Stewart, Ph.D., Chair

David A. Roberson, Ph.D.

Pavana Prabhakar, Ph.D.

Charles Ambler, Ph.D.
Dean of the Graduate School

Dedication

Dedicated to my parents.

Md. Israrul Haque and ***Shahnaz Haque***

"God bless our family"

AN IMPROVED SIN-HYPERBOLIC CONSTITUTIVE MODEL FOR CREEP DEFORMATION AND DAMAGE

by

MOHAMMAD SHAFINUL HAQUE, B.Sc.

THESIS

Presented to the Faculty of the Graduate School of

The University of Texas at El Paso

in Partial Fulfillment

of the Requirements

for the Degree of

MASTER OF SCIENCE

Department of Mechanical Engineering

THE UNIVERSITY OF TEXAS AT EL PASO

May 2015

Acknowledgements

I would like to thank my advisor Dr. Calvin M Stewart for his teaching, training, guidance, thoughtful suggestions, and support throughout my graduate education. My thanks goes to the member of my thesis committee, who are: Dr. David A Roberson, Dr. Pavana Prabhakar.

I would like to thank all my colleagues, all the people who have provided technical, emotional, or spiritual support during my studies including Graduate School, ME Front-Desk and OIP (Office of International Program).

Abstract

Inspection and maintenance of industrial gas turbines (IGTs) cost millions of dollars. Growing demand of obtaining higher IGT efficiency leads to higher temperature and pressure operating conditions. Long exposure of turbine components at elevated temperature and pressure makes creep damage critically important to consider during planning, designing and operating conditions. Effective and economic maintenance requires accurate creep deformation, damage evolution and rupture life prediction information. Creep prediction models are used to determine the state of the turbine components and to schedule the inspection, maintenance and replacement time periods. The more accurate the prediction model, the less is the overall cost by the reduction of over maintenance, lay off time and premature replacement of components. There are many popular models available for each of these creep phenomena. Different models are developed on different assumptions. Use of different models to predict these phenomena may lead to inconsistent creep prediction. It is very important to have one set of constitutive equations that can predict all these creep phenomena. At the same time, the set of equations has to be accurate and easy for application. In the present work an improved Sin-hyperbolic (Sinh) model is introduced. Analytical derivation, numerical analysis and FEM simulations are performed to characterize the capacity to predict creep deformation, damage evolution and creep rupture life. Comparison with other popular models, scope of applicability, advantages over other models and limitations are discussed in detail. Experimental data collected from literature for 304 Stainless Steel (SS) of creep deformation and creep rupture are used to compare the Sinh model with other models at different level of temperature and stress. A process to determine the material constants of both models is clearly elucidated. The results and experimental data fitting curves produced by these model shows that the sinh model produces a continuous damage (from zero to unity) by normalizing the experimental data. It is found that overall the new Sinh model offers more flexibility and prediction accuracy. FEM simulations on notched specimen are conducted. Notches enable the ability to study the effect of stress concentration evolution of creep damage

and rupture in components during life prediction modeling. Numerical analysis on notched specimen can provide prediction of creep damage or crack propagation of materials containing defects or initial cracks. In this work, the Sin-hyperbolic (Sinh) model is demonstrated to significantly mitigate mesh dependency and exhibits a nonlocal damage distribution around the crack when compared to the other classical model. Prediction model equations are implemented into FORTRAN using ANSYS Mechanical APLD (ANSYS Parametric Design Language) code to perform the analysis. USERMAT (user material routine) of ANSYS UPF (user-programmable feature) is used to define the mechanical constitutive behavior and stress-strain relations. Finite element analysis of circular notched specimen of 304 Stainless-Steel (SS) show that the Sinh model overcomes the mesh dependency problem, converges to a unique result upon mesh element refinement. Constant load is applied and the modulus of elasticity is degraded as crack propagates with each time steps. Elastic modulus decreases with damage increment and accelerates deformation. A series of simulation at different mesh size are used to check the mesh dependency. Results of single element FEM analysis are matched with experimental data collected from literature to validate the model constants and iteration accuracy. Contour plots of damage evolution, and mesh dependency of crack growth rate are discussed in detail. It is demonstrated that the Sinh model offers better creep damage, and crack growth analysis and significantly improves the stress sensitivity, damage localization, and mesh-dependency of numerical results.

Table of Contents

List of Tables

List of Figures

Chapter 1: Introduction

1.1 MOTIVATION

Industrial gas turbine (IGTs) [Figure 1.1-1.2] components may fail due to vibration, fatigue, foreign object damage, environmental attack, corrosion, erosion, embrittlement, sulphidation and creep. Combined effect of all these issue leads to damage of turbine components **[1**],**[3]**. It is reported that combined effect of all these damage mechanism initiates creep-fatigue (constant loading) or thermomechanical fatigue (dynamic thermal loading) failure mechanism. These two mechanism are the principal cause of microstructureal damage **[5]**. U.S air force makes an expenditure budget of $100 million per year to inspect and fix high cycle fatigue problem **[1]**. High operating temperature & pressure, mechanical & thermal stress are the driving force of creep failure [**4**],[**5]**. Dundas **[6]** indicated an statistics saying that 62% of the total damage cost of gas turbines are consists of cycle cooling, fatigue, creep and surge related failure. 19% of the heavy duty gas turbine damage costs are due to creep damage. Components operating under high stress and temperature are susceptible of creep. Creep is gradual deformation, distortion or elongation of the components, that can lead to failure. It is stated that, an increment of as small as 15°C operating temperature, cuts the components creep life by 50% **[1]**. Modern IGTs experiences operating conditions of over 18 pressure ration and temperature above 1425°C [**8]**. Long time exposure of turbine components to high temperature changes the morphology of the gamma prime phase, resulting loss of material creep strength **[1]**. Growing demand for higher efficiency requires higher operating temperature and pressure. Creep life study becomes critical to avoid failure and a key feature in designing components. Turbine hot section components comprise 50-70 % of the maintenance cost for gas turbine operation **[3]**. Though rotating parts are more susceptible to creep damage, real life statistics shows that stationary components are also susceptible to creep damage. Bloch **[7]** stated that rotor and blades are consists 28% of primary cause of gas turbine failure. Stationary components and nozzles consists 18% of the failure cause. Turbine components [Figure 1.2] are primarily made

of superalloys. Iron based superalloys got replaced by nickel based and cobalt based superalloys. Iron based superalloy made components can be found in some old turbines or in cold section components.

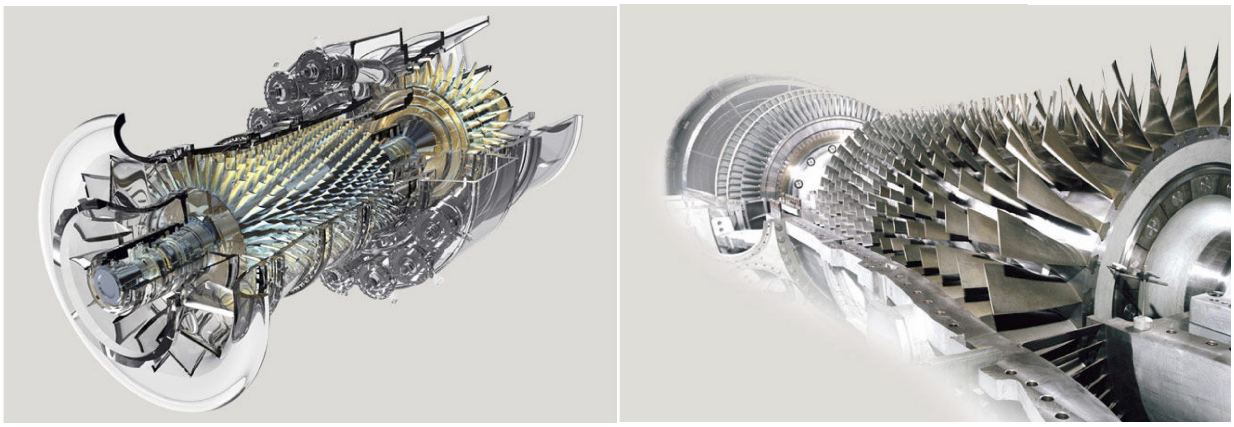

Figure 1.1: GE Heavy duty gas turbine (50 Hz, 391 MW)

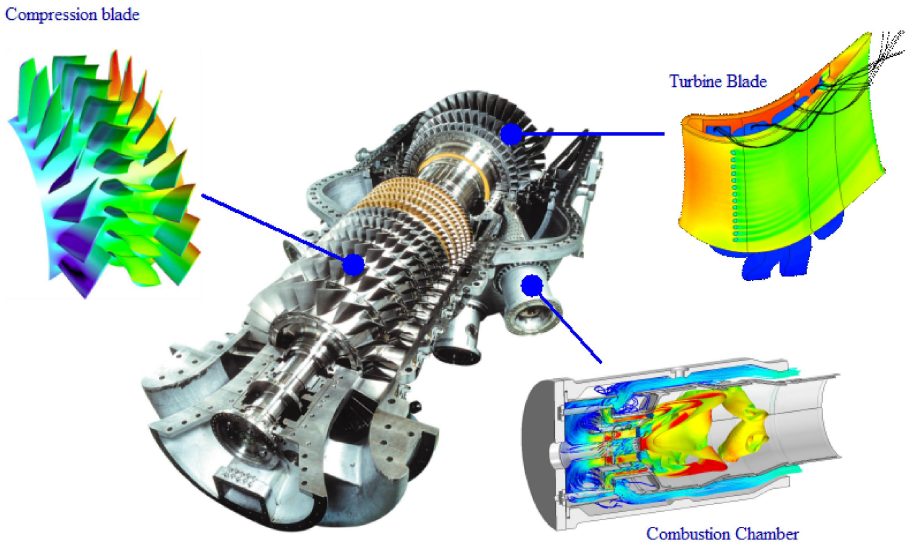

Figure 1.2: Kawasaki Heavy Industrial Gas Turbine (L20A)

These are called "super" because they contain so many alloying elements and due to their good mechanical properties at high as well as low temperature. Most of the hot components are made of nickel based super alloy because of its comparatively greater strength. Cobalt based super

alloys are used for vanes due to their good weldability and resistance to hot corrosion [**3**]. In spite of good mechanical properties of these super alloys, (with or without protective coating) they are still susceptible to creep damage. During creep, material elongates due to tensile stress. This creep deformation may lead to tip rub. On cooling blade, tip rub may block the cooling air

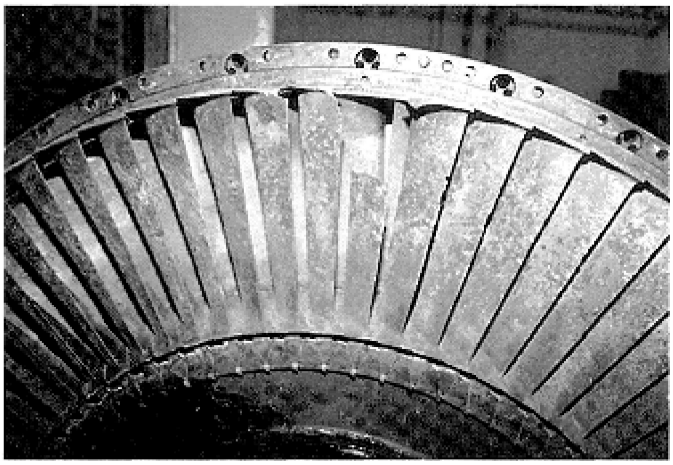

Figure 1.3: Combined failure due to tip rub (due to creep), corrosion and fatigue [1]

Figure 1.4: Creep Damage of turbine blade (Berkeley Research Company, Berkeley California)

Figure 1.5: Forced outage of IGT [**5**]

flow, resulting over heating of the blades [**1**],[**3**]. Excessive creep deformation may lead to contact of blade tip with the turbine body causing collateral damage [**5**]. Apart from total failure, IGTs inspection and maintenance cost are affected by creep deformation. Original equipment manufacturer (OEM) stated that combustion inspection occurs every 12000 hours that costs approximately 1.66 million dollars. Major inspection occurs at 100,000 hours that costs 0.24 million dollars [**9**]. Effective and economic inspection and maintenance can save millions of dollars to the investors. Accurate creep damage prediction model can optimize the inspection time and reduce lay off costs. Inaccurate prediction of creep life may lead to over design of turbine components that leads to poor overall efficiency. Service and maintenance engineers are doing premature servicing of components and early replacement of components to avoid failure. More accurate and easily applicable creep deformation are needed to avoid this problems.

1.2 RESEARCH OBJECTIVES

The objective of the research is to improve a novel sin-hyperbolic creep deformation and damage model. The goals of the research is

Improvement of the sinh model

Background study of existing popular creep model are conducted. Limitations of existing popular model are discussed. Advantages of sinh model are discussed analytically and numerically. Characteristics of the model, steps in fittings with experimental data are discussed in detail.

Numerical analysis

Experimental data collected from literature are used to determine the constants for this model. Comparison with other popular model is discussed in detail. Advantages over other models are examined.

FEM simulation

A series of finite element simulation on notched specimen is conducted. ANSYS mechanical apdl is used.

1.3 ORGANIZATION

The present work is organized as follows. Chapter 2 introduces with the creep deformation and damage literature review. Popular model are used to with fit experimental data to understand the characteristics of the models and to study possible improvement. Chapter 3 simply introduces the material used in this study. Chapter 4 discusses the popular Kachanov-Rabotnov model, its limitations in detail. Introduces the novel sinh model. Advantages of sinh model is discussed. Chapter 5 contains the numerical analysis of the Kachanov-Rabotnov model and the sinh model. Experimental data collected from literature is are used to determine the constants of each model. Graphical comparison and detail discussion is presented. Chapter 6 covers the finite element study of the sinh model. FEM simulation using ANSYS software are conducted for sinh and Kachanov-Rabotnov model. Detail comparison and discussion of this two model is provided. Finally chapter 7 contains the conclusions and the future study.

Chapter 2: Background

2.1 INTRODUCTION

Towards the improvement of the sinh model. Study of creep and popular creep model must be conducted that will provide the basic idea of a typical model. Background study provides the information about current stage of this field. Problems and limitations can be understand from background study that makes the way for possible improvement. This section includes the early stage creep rupture life prediction models. Alongside with the study, experimental data fitting capacity of the model is performed.

2.2 CREEP

Creep is time dependent deformation characterized by slow inelastic flow of material, behaving like viscous **[10]**. Creep dominant deformation occurs at temperature level $0.4T_m < T < T_m$. Primarily creep is dependent on temperature, time, loading rate, applied stress, and shape of the components. Time dependence implies that the rate of deformation is significant that time should be considered during engineering assumptions. Vicat conducted the first experiment to assess creep phenomena [**10**]. In 1910, Andrade divided the creep deformation into three stages and proposed a law for primary creep [**11**]. Figure 2.2 shows the three stages of creep deformation. Primary, secondary and tertiary stages. The first primary stage is short lived phenomena for superalloys, deformation at this stage is considered small compared to total deformation and can be neglected in constitutive modeling. It initially has high creep strain rate and gradually decelerates. And finally becomes stable at steady state creep rate. Secondary or steady state creep rate is the second creep stage. It has almost constant strain rate due to balance between strain hardening and recovery mechanics. Nucleation of grain boundary and grain boundary sliding takes place in this region. in stage three, accelerated creep rate is observed that finally leads to failure. This stage can be realized by net area reduction due to elongation, evolution of voids, micro-cracks, defects takes place, leading to rupture.

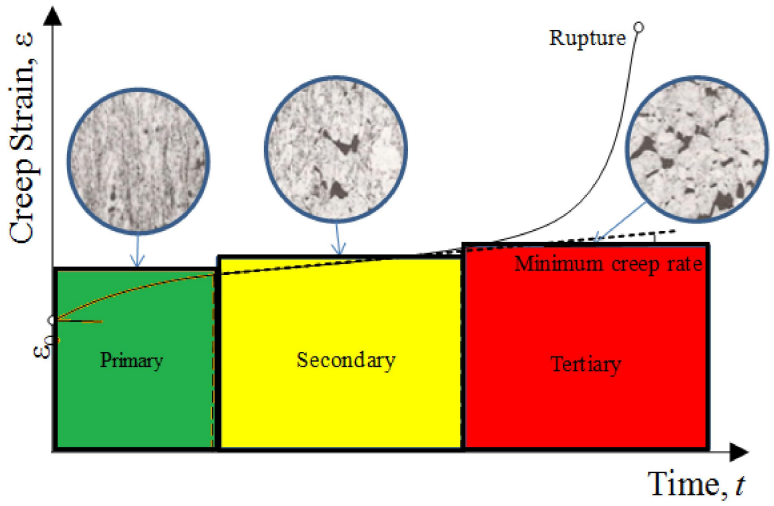

Figure 2.1: Three stages of creep deformation [**5**]

In 1980 Kraus [**12**] some futures that should have in materials to possess a good creep resistance. The creep resistance properties are:

- Metallurgical stability under long term high temperature exposure
- Resistance to oxidation and corrosive media
- Larger grain size that reduces the grain boundaries (At grain boundaries most of the creep deformation takes place, less grain boundary will minimize the risk to creep deformation)

2.2.1 Creep Rupture Prediction Approaches

There are many approaches available to model creep rupture life. Some approaches are listed in the Table 2.1.

Table 2.1: Creep rupture life prediction model

Source	Model
Larson-Miller, 1952	$LMP = T(\log(t_r) + C)$
Manson-Hafard, 1953	$MHP = \frac{\log t_r - \log t_a}{T - T_a}$
Orr-Sherby-Dorn, 1954	$\ln t_r - \frac{Q}{k * T} = OSDP$
Graham-Walles, 1955	$\theta = t \cdot (T' - T)^{-A}$
Monkman-Grant, 1956	$\log(t_r) + m \cdot \log(\dot{\varepsilon}_{min}) = k_{MG}$

Larson-Miller Approach

Larson-Miller approach (1952) is the earliest method for extrapolating creep rupture life from short term experimental data for constant engineering stress. It is assumed that Arrhenius equation is related to creep rate [**12**].

$$\frac{d\varepsilon}{dt} = A\exp(-\frac{\Delta H}{RT}) \tag{1.1}$$

Where A is a constant, ΔH is the activation energy for creep processes, R is the gas constant and T is the temperature. Further it is assumed that minimum creep rate is inversely proportional to rupture life:

$$t_r * (\frac{d\varepsilon}{dt})_{min} = \text{constant} \tag{1.2}$$

Thus the Larson-Miller model only the secondary or steady state creep rate & neglects the primary and tertiary creep regimes. Applicability of Larson-Miller approach can be checked if creep-time/temperature data follows equation (1.2). From Eq. (1.1) and (1.2) we get

$$t_r * A * \exp(-\frac{\Delta H}{RT}) = \text{constant} \tag{1.3}$$

Again it is assumed that ΔH(activation energy) is dependent on applied stress, now taking logarithms of both side gives [**15**]

$$\log_{10} t_r + \log_{10}(\exp - \frac{\Delta H}{RT}) = \log_{10}(\frac{\text{constant}}{A}) \tag{1.4}$$

$$T*(\log_{10} t_r + C) = 0.434\frac{\Delta H}{R} \tag{1.5}$$

Assuming, $\log_{10}(\frac{\text{constant}}{A}) = C$, thus C depends on the Arrhenius constant (A) and fracture-strain constant, so C depends on the material property but dependence of material property is very minimum because of its logarithm dependency thus C value should be fixed for a type of material of limited range [**15**], Finally the Larson-Miller approach can be written as:

$$LMP = T(\log t_r + c) \tag{1.6}$$

where T is temperature in Kelvin (K), t_r is rupture time, C is a constant, and LMP is the Larson-Miller parameter a function of stress.

$$LMP = 0.434\frac{\Delta H}{R} = f(\sigma) \tag{1.7}$$

As Larson-Miller is based on constant creep rate so the dependency of LMP on stress function is fixed thus particle-coarsening, void-coalescence is neglected and the primary creep has to be brief it cannot be dominating [**15**]. Historically for metals, C can be equal to 20 however, Fixing C=20 is no longer acceptable in the research. Furillo **[16]** et. al. reported C values ranging from 10 to 50 in many cases of metal alloys. Vasudevan [**17**] et. al. reported they have found C value 13.5 for austenitic stainless steel. When LMP is set up as a function of applied stress [Eq. (1.4)] C valued is determined by experimental data fitting analysis. Rupture time can be predicted by [Eq. (1.5)] to the following form (given that operating temperature is known).

$$t_r = 10^{(LMP - T*c)/T} \tag{1.8}$$

So for Larson-miller it is need to evaluate only two parameter, the value of C and LMP (which has to be define as a function of stress). Naturally to collect experimental data test is run operating condition at high temperature and low stress to conduct short-term test and use these data sets to extrapolate long term creep life. Though a lot of uncertainties goes in creep deformation yet the Larson-Miller method works well.

Larson-Miller constant C:

One way to evaluate the value of C is to rearranging the Larson-Miller equation in $y = m*x + c$ form where x and y are the value of x-axis and y-axis sequentially and m is the slope of the curve and c is a constant. Thus $\log_{10} t_r = LMP * \frac{1}{T} - C$ can be plotted as lines of $\log_{10} t_r$ versus $\frac{1}{T}$ for constant stress. So at least two data set at constant stress but different temperature is needed to generate one straight line. Now if the line is extended to the $\log_{10} t_r$ axis the intersection will give the value of C. To make it more accurate more different line can be obtained by plotting different data sets at different stress condition and all the lines will coincide at same point [Figure 2.2].

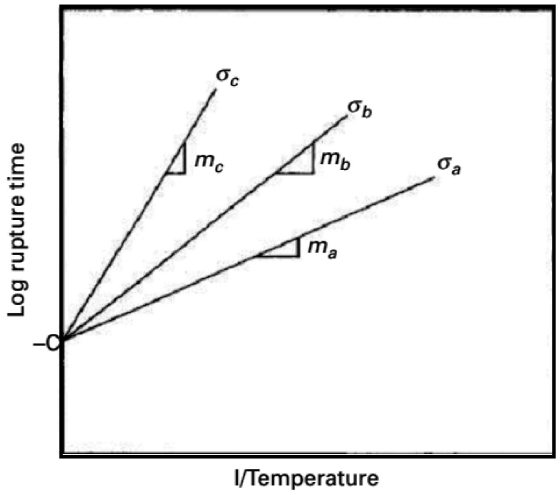

Figure 2.2: log rupture time vs inverse temperature curve for Larson-Miller model

The other way to evaluate the value of C is regression analysis, for this the many experimental data used the more confident C value can be obtained. All fourteen data sets are used to calculate the LMP at different C value. Staring from C=20 and varied in range of 18.5 to 20.5 the MATLAB curve fitting directed that minimum residual is observed at C=19. During fitting it was observed that the difference between maximum and minimum LMP values remains the same for all C values. The later way is used here because in Larson-Miller the rupture time depends on C value by power of ten [eq. (1.5)] so slight change in C value can lead to high overestimation during extrapolation. So if graphical plot is used it is more likely to get deviated value of C, plus in real life experimental data plots does not coincide at one point thus it is more difficult to evaluate correctly by graphical method.

The LMP function:

After selecting the *C* value the LMP values evaluated from experimental data were plotted against applied stress and the EUREQA [**19**] symbolic regression software was used to find an equation of LMP versus applied stress. EUREQA fits [Equation (1.4)] as best fit.

$$\mathrm{LMP}(\sigma) = 31250 + 41.86*\sigma - 1491.92*\mathrm{SQRT}(\sigma) \tag{1.9}$$

Figure 2.3 shows that experimental data sets are well around the model LMP function [equation (6)].

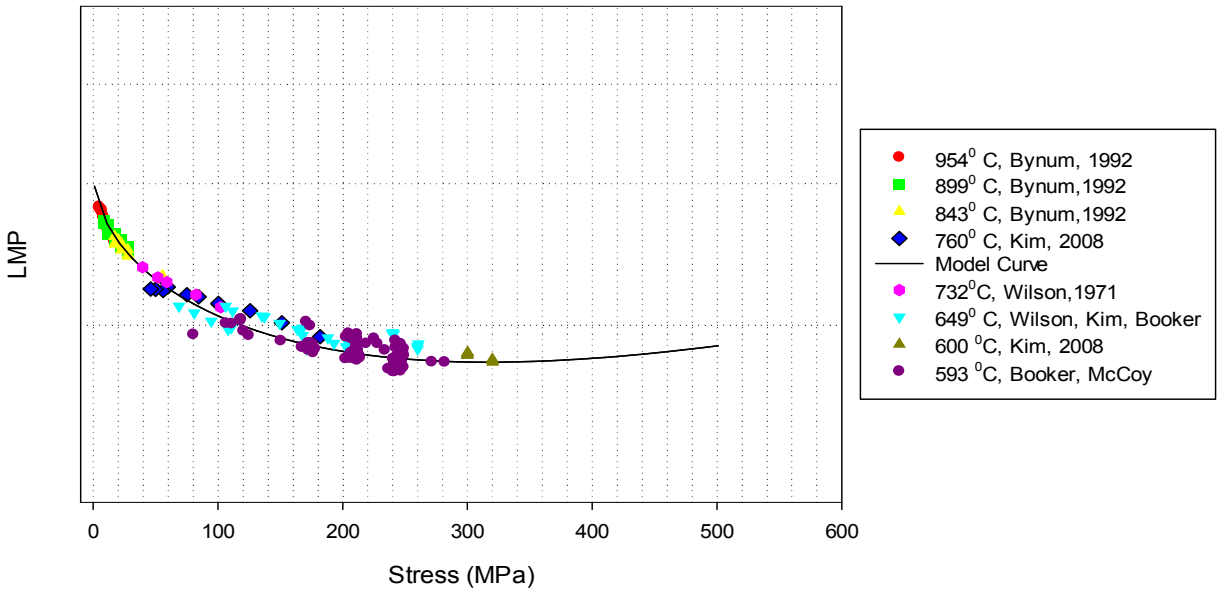

Figure 2.3: LMP vs Applied Stress. The points represents the LMP values at different temperature and the line represents the developed model.

DiMelfi [18] states that [Equation (1.4)] can take any form but the most popular form is a polynomial. While generating an universal form of LMP equation (as fourteen data sets of different time, temperature and stress is used) it was found that the new form [Equation (1.6)] gives much better prediction of LMP. The polynomial equation gives less accurate predictions compares to the square root equation because in the Larson-Miller equation the LMP value acts as a power of ten. Small deviation in LMP leads to very large deviation in life prediction.

[Figure 2.5] shows that the Larson-Miller model fits the experimental data. However at very low temperature and very high stress (near to UTS) the curve cannot predict the rupture life. For the new square root equation the first derivative is

$$\frac{d(LMP)}{d\sigma} = a_1 + a_2 * 0.5 * \sigma^{-0.5} \qquad (1.10)$$

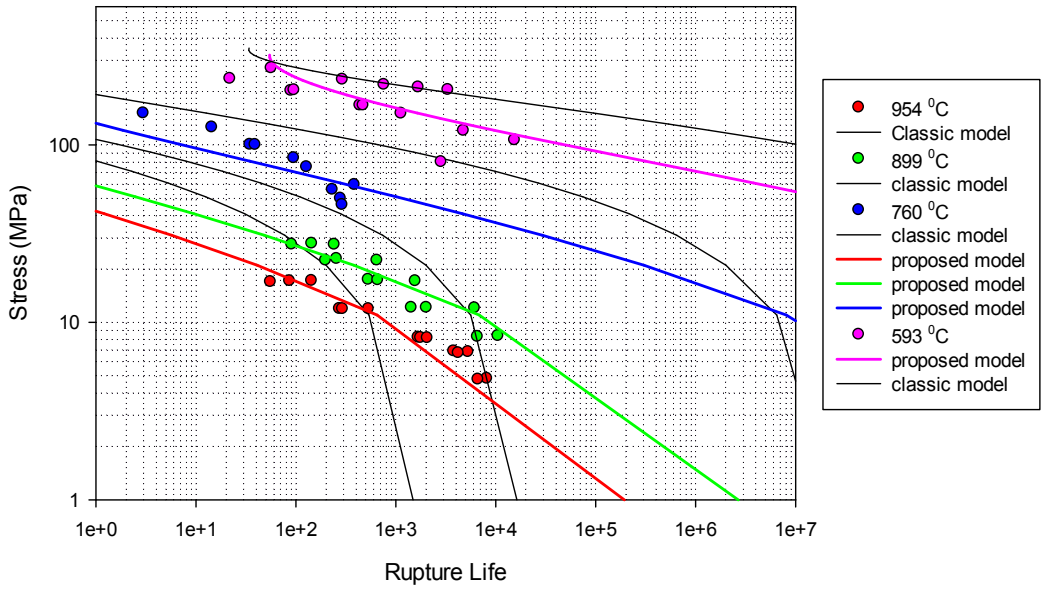

Figure 2.4: Comparison between the LMP function as polynomial form (black lines) and new square root form (color lines). It is evident that square root form fits the experimental data better.

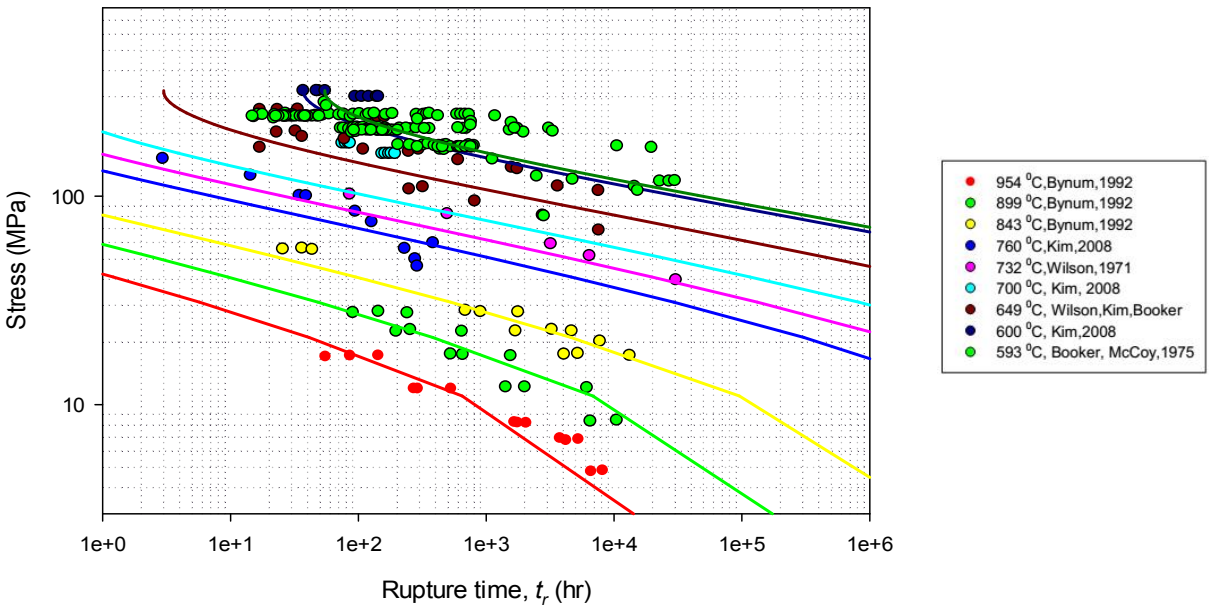

Figure 2.5: Stress Vs Rupture time. By using [Equation (5) and (6)]. The solid lines are modeled curve and the dot points are experimental data.

Setting the derivative equal to zero (where the curve will reach at maximum point) and solving for σ results is $\sigma = 317.56\text{MPa}$, The model has a inflection point at 317.56 MPa which results in fictitious prediction of life above this stress value. To avoid this limitation a new approach is planned [Equation (1.6)]. where *n* is function of temperature

$$stress = \frac{a}{time^{n} + b} \tag{1.11}$$

and the ratio (*a/b*) determines the maximum stress applicable (which is the Ultimate tensile strength (UTS)) and will be treated as a function of temperature, $a/b = f(\text{T})$ [Figure. 2.6]. The main advantage is it will generalize the model from UTS to low stress (where life will be theoretically infinite), unlike Larson-Miller approach, this model will use UTS as a function of temperature ($\text{UTS} = f(\text{T})$), means the UTS will be different for same material at different temperature which will give the safe operating stress limit for that specific temperature.

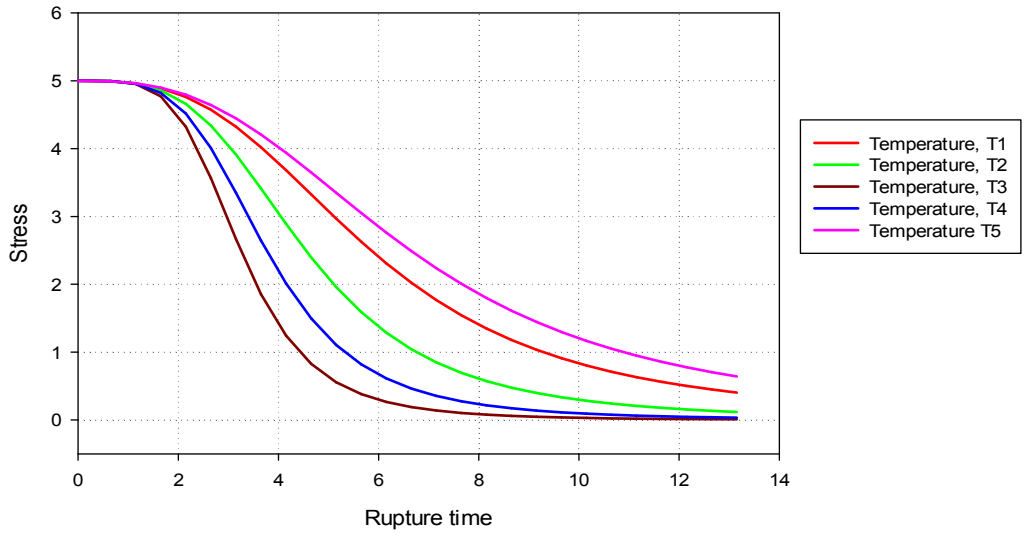

Figure 2.6: Planned stress vs rupture life model curve

Manson-Haferd:

In 1953 Manson-Haferd [20] proposed a time-temperature parameter based on experimental data analysis avoiding the physical theory. They refers creep rupture value by following equation:

$$MHP = \frac{\log t_r - \log t_a}{T - T_a} = f(\sigma) \tag{1.12}$$

here, MHP is the Manson-Haferd parameter , t_r is the rupture time in hour, T is temperature in Kelvin, t_a & T_a are constants. The stress function is usually given by forth order polynomial in $\log(\sigma)$ [21].

$$f(\sigma) = a_0 + a_1 * (\log \sigma) + a_2 * (\log \sigma)^2 + a_3 * (\log \sigma)^3 + a_4 * (\log \sigma)^4 \tag{1.13}$$

Later in 1968 Manson [**10**] to reduce the exceedingly optimistic values for rupture life by Larson-Miller and to reduce pessimistic values of Manson-Haferd model he gave a mixed parameter

$$\log t_r + \frac{(\log t_r)^2}{40} - \frac{40000}{T} = m \tag{1.14}$$

here, m is the parameter.

In ideal situation all extrapolated iso-stress lines intersects at one point [Figure 2.7] other than the axis having coordinates ($\log t_a$ and T_a). These two are the constants for Manson-Haferd model which varies depending on the materials type. It is also reported that these constant set ($\log t_a$ and T_a) is not randomly distributed but has a linear correlation with high coefficient of 0.995 [11]. Having two constant to evaluate it is more complicated than Larson-Miller model as for Larson-Miller only one constant *C* is required to evaluate. [Figure 2.7] is unlike the [Figure 2.2] of the Larson-Miller in sense that Larson-Miller model expresses $\log t_r$ as a function of reciprocal of temperature (1/T) but Manson-Haferd approach expresses as a function of straight temperature [12].

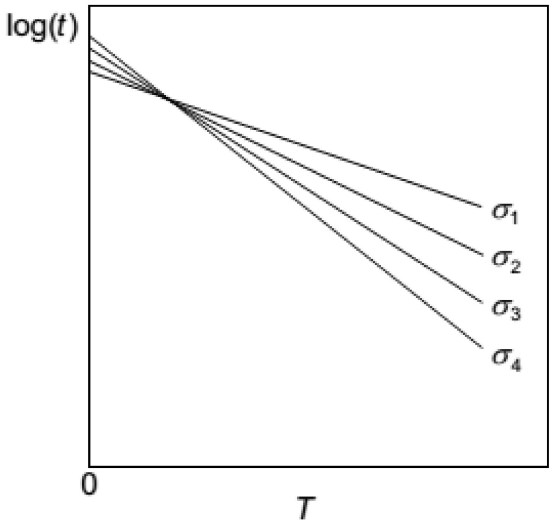

Figure 2.7: Manson-Haferd Creep model (Ideal case) [**10**]

In reality the iso-stress lines does not intersects at one point but has several interactions [21]. Plus, curve plotting for large number of data set and extrapolation them to intersect is more time consuming [**62**]. In order to by pass this problem regression analysis is done and optimum constant set was selected at possible high value of R^2. The optimum value (log t_a = 19.62 and T_a=350) is selected at R^2=0.93. Using this constants a polynomial function is obtained using EURICA[**19**] software where MHP is a dependent on only applied stress.

$$MHP = f(\sigma) = 2.159*10^{-7} * stress^2 - 1.19*10^{-4} * stress - 0.0182 \quad (1.15)$$

Figure 2.8 shows that the experimental MHP is well distributed round the modeled MHP as a function of applied stress. And [Figure 2.9] shows that model creep rupture prediction for Manson-Haferd approach are in touch with the experimental data.

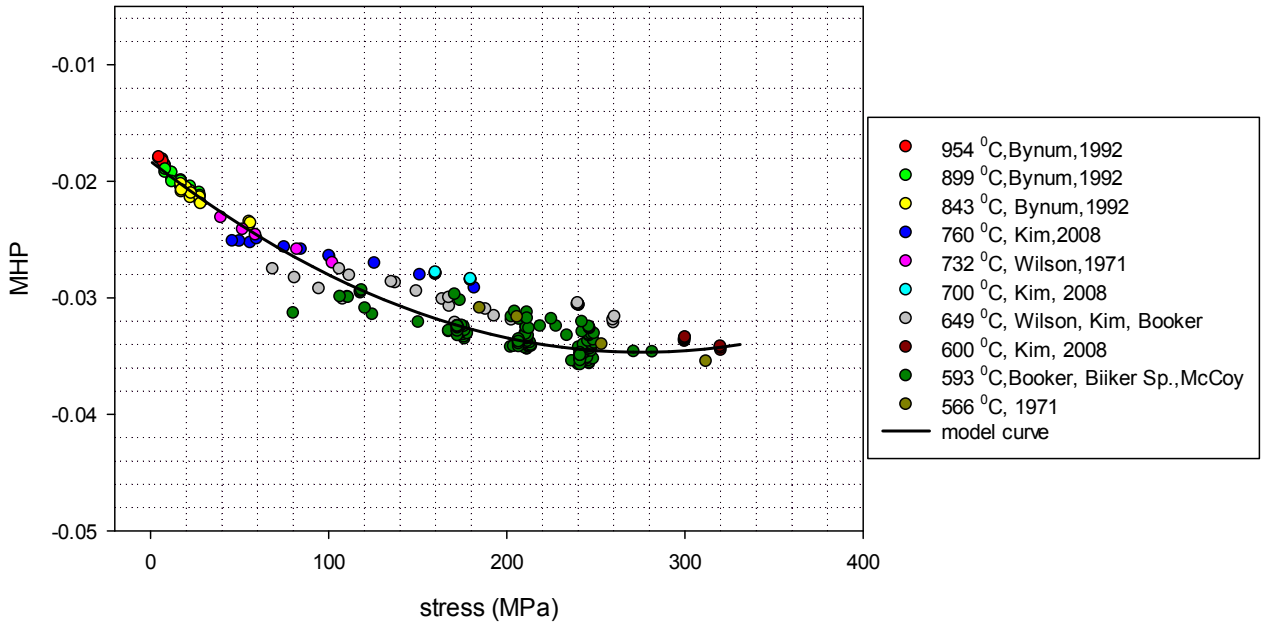

Figure 2.8: MHP vs applied stress

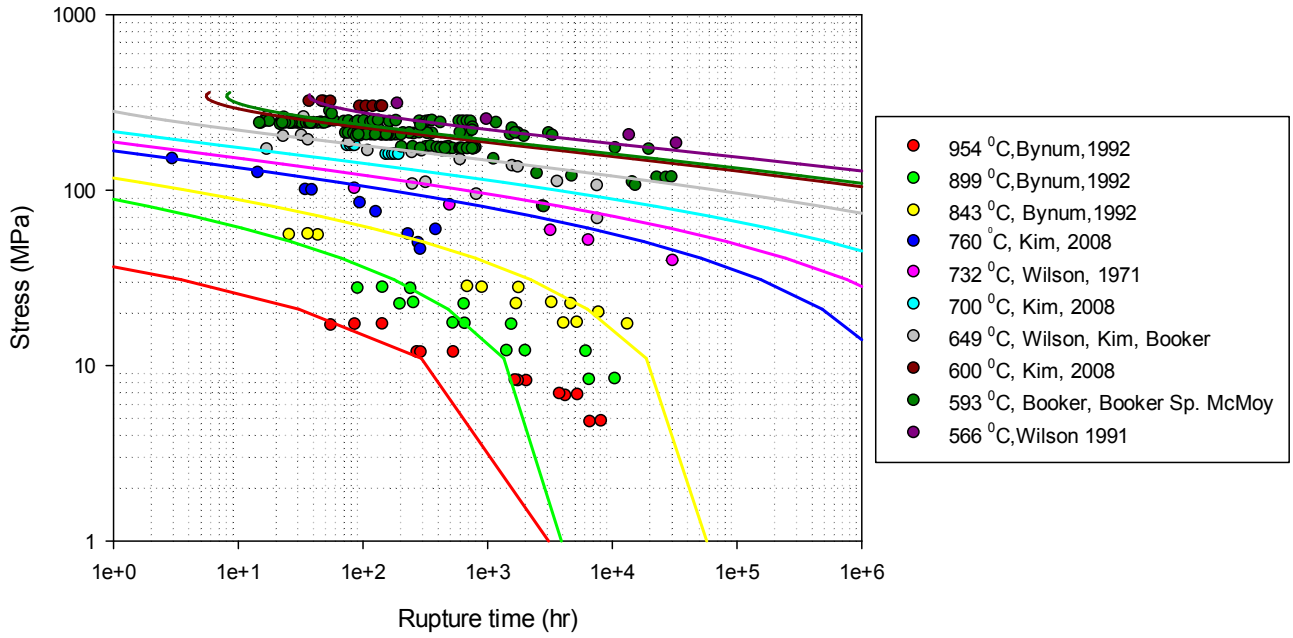

Figure 2.9: stress vs rupture time curve (experimental data and the model curve)

Orr-Sherby-Dorn Method (OSD):

Based on fundamental study conducted by Sherby et. al. they found following relation [**10**]

$$\ln t_r - \frac{Q}{k*T} = OSDP \tag{1.16}$$

Q is the activation energy of diffusion or creep, t_r is the time to rupture and OSDP is the Orr-Sherby-Dorn parameter. It is different from Larson-Miller in that the iso-stress lines are parallel. But it can be shown that OSD method can be derived same way as Larson-Miller and the difference for iso-stress lines is due to assumptions.

<table>
<tr><td colspan="2">Parallel derivation of Larson-Miller and Orr-Sherby-Dorn method:</td></tr>
<tr><td colspan="2">Secondary or steady state creep rate assumption:
$$t_r * (\frac{d\varepsilon}{dt})_{\min} = k(\text{constant})$$ (a)</td></tr>
<tr><td colspan="2">Arrhenius equation related to creep rate:
$$\frac{d\varepsilon}{dt} = A\exp(-\frac{Q}{RT})$$ (b)</td></tr>
<tr><td colspan="2">Putting eqtn. (b) into eqtn. (a) we get:
$$\exp(-Q/R*T)*t_r = \frac{k}{A}$$
Taking log on both side :
$$\log t_r - 0.43*\frac{Q}{R*T} = \log\frac{k}{A}$$</td></tr>
<tr><td>Larson-Miller assumed that $Q = f(\sigma)$ and
$\frac{k}{A} = \text{constant}$,
Thus, $LMP = \frac{0.43*Q}{R} = f(\sigma)$
So, $\log t_r - \frac{LMP}{T} = C, (\text{constant})$</td><td>Sherby assumes that $A = f(\sigma)$ and
$0.43*\frac{Q}{R*T} = \text{constant}$,
Thus, $OSDP = \log\frac{k}{A} = f(\sigma)$
So, $\log t_r - \frac{0.43*Q}{k}*\frac{1}{T} = OSDP$</td></tr>
<tr><td>Now if we plot the above equation we get</td><td>Now if we plot the above equation we get</td></tr>
</table>

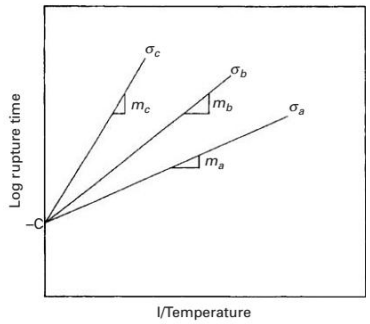	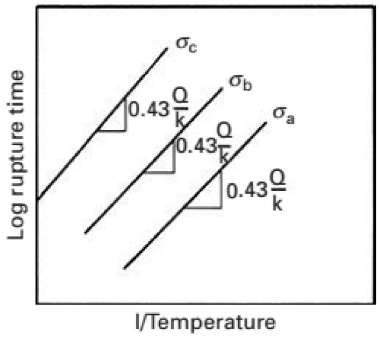
Rearranging: $LMP = T(\log t_r + c)$	Rearranging: $2.3*(\log t_r - OSDP) = \frac{Q}{k*T}$ converting into natural logarithm: $\ln t_r - \frac{Q}{k*T} = OSDP$

2.2.2 CONSTITUTIVE MODEL FOR CREEP STAGES

In 1954, Or et al introduced that activation energy for creep and diffusion are same for more that 25 metals.

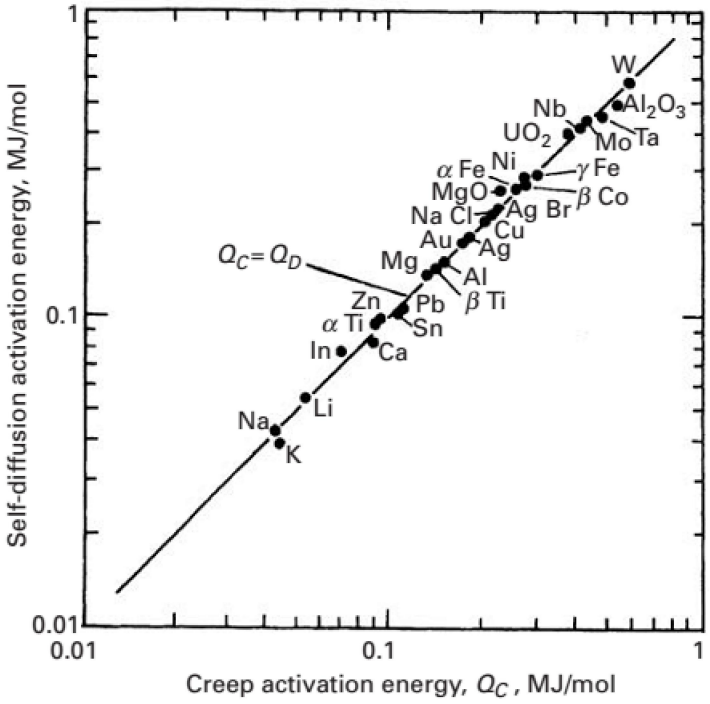

Figure 2.10: Linear relation between Diffusion and Creep activation energy [**10**]

Creep can be divided into two mechanisms: diffusion creep and dislocation creep. In diffusion creep two mechanism are important. Nabarro-Hering and Cobel mechanisms. In Nabarro-Hering mechanisms flux of vacancies inside the grain moves such a way that length of grain increases along the direction of applied load. Coble proposed the second mechanism diffusion of grain boundaries instead of the bulk. In dislocation (or Power Law) creep, dislocation glide takes place aided by vacancy diffusion [10]. Some early stage primary and secondary constitutive creep model are listed in Table 2.2 and Table 2.3.

Table 2.2: Primary creep constitutive equations [**12**]

Source	Creep Law
Andrade, 1910	$\varepsilon_{cr} = (1 + A\,\mathrm{t}^{1/q})\exp(\mathrm{kt}) - 1$ $\varepsilon_{cr} = A\,\mathrm{t}^{1/q}(\mathrm{t} \to 0, \mathrm{k} \to 0)$
Baily, 1935	$\varepsilon_{cr} = Ft^{n}(\frac{1}{3} \le \mathrm{n} \le \frac{1}{2})$
McVetty, 1943	$\varepsilon_{cr} = G(1 - e^{-qt}) + Ht$
Graham and Walles, 1955	$\varepsilon_{cr} = \sum_{i} a_i t^{n_i}$

Table 2.3: Secondary Creep constitutive equations [**5**]

Source	Creep law
Norton, 1929	$\dot{\varepsilon}_{cr} = A(\sigma / \sigma_0)^{n}$
Soderberg, 1936	$\dot{\varepsilon} = A\{\exp(\sigma / \sigma_o) - 1\}$
MCVetty, 1943	$\dot{\varepsilon}_{cr} = A\sinh(\sigma / \sigma_0)$
Dorn, 1955	$\dot{\varepsilon}_{cr} = A\exp(\sigma / \sigma_0)$
Johnson, Henderson, and Khan, 963	$\dot{\varepsilon} = A_1(\sigma / \sigma_0)^{n_1} + A_2(\sigma / \sigma_0)^{n_2}$
Garofalo, 1965	$\dot{\varepsilon}_{cr} = A\{\sinh(\sigma / \sigma_0)\}^{n}$

Theta projection model

It is a multistage model. This model consists of two term, first term models the primary creep and the last term models the tertiary creep. M. Law et. al stated three reasons to name theta projection model as most useful. The Theta projection model is more useful for analyzing creep data than other current model is for three reasons. First, it can generate data that conveniently models stress and temperature changes. Secondly, the Theta projection allows estimates of the minimum creep rate from the four theta constant values. Few other available equation systems describe creep curves accurately. Thirdly, the Theta projection can be used to make a reliable estimate of the remaining life of a material undergoing creep [**60**].

$$\varepsilon_r = \theta_1(1-e^{-\theta_2 t_r}) + \theta_3(e^{\theta_4 t_r} - 1) \tag{1.17}$$

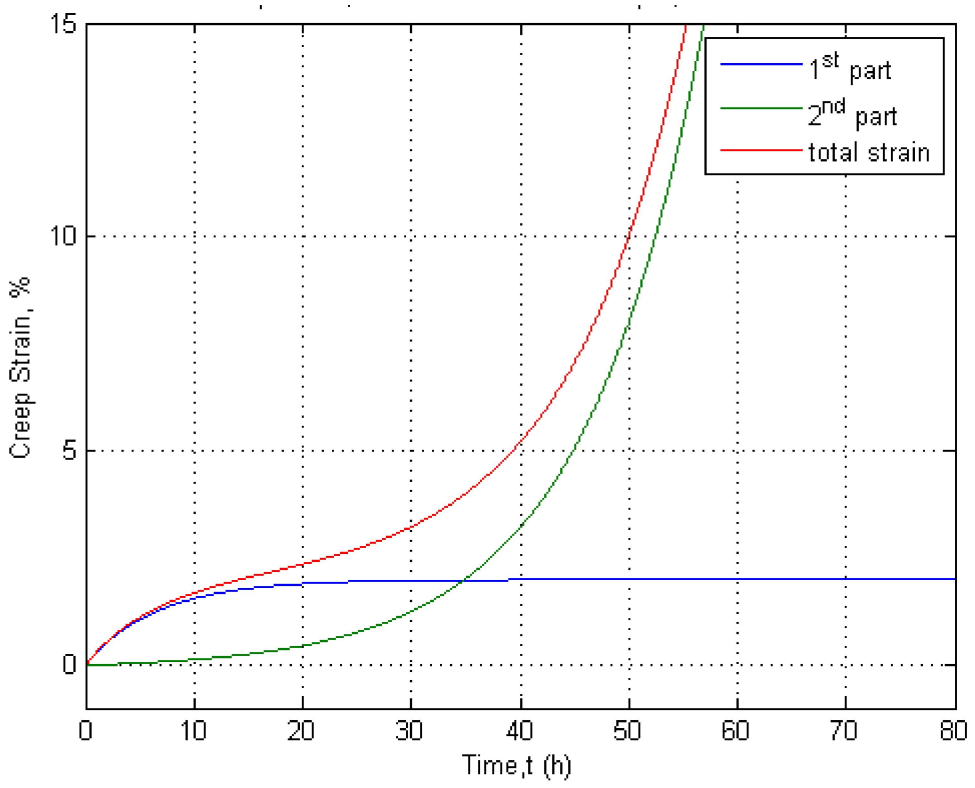

Figure 2.11: Construction of Theta projection model

Figure 2.11 shows the characteristics assumptions of theta projection model. The blue line represents the primary creep (first term of the equation) that becomes stable after initiation

of secondary stage. The green line represents the tertiary creep regime (second term of the model). While the addition of this two term accommodates the secondary creep regime. Finally, tertiary creep damage takes over leads to failure.

Chapter 3: Material

304 stainless steel is the most versatile and widely used stainless steel. Experimental data are collected for 304 SS that reduces the need of mechanical tests. 304 SS is used in making turbine components.

Table 3.1: Typical chemical composition of 304 SS [**61**]

304 SS	**C**	**Mn**	**Si**	**P**	**S**	**Cr**	**Ni**	**N**
%	0.08 max	2.0	0.75	0.045	0.03	18-20	10.5	0.1

304 is high corrosion resistant, high ductility, excellent drawing, forming, and spinning properties. Upon cold work non magnetic 304 SS may become slightly magnetic. At room temperature 304 SS ultimate tensile stress is 621 MPa and yield stress 290 MPa. 304 SS can be exposed up to 899°C without any oxidation scaling. 304 SS is non-hardenable by heat treatment due to very low carbon presence. Typical annealing temperature is (1038-1121)°C. For annealing purpose thin metal section may be air cooled but for heavy section the specimen should be water quenched. This type of metal is highly draw able. Their combination of low yield strength and high elongation percentage (50-55%) makes is successful in complex shaping. After forming parts should be fully annealed as soon as possible. 304 stainless steel is generally considered to be weldable by the common fusion and resistance methods.

Table 3.2: Typical Mechanical Properties of 304 SS [**61**]

	UTS (MPa)	**YS (MPa)**	**Elongation %**	**Brinell**
304 SS	621	290	50-60	B 80-99

Chapter 4: Creep Damage Constitutive Model

When subject to a high temperature and pressure environment, 304 stainless steel (SS) is susceptible to creep deformation despite having high temperature strength, toughness and resistance to degradation in corrosive or oxidizing environments. 304 SS shows strain rate-sensitivity and exhibits creep deformation at room temperature [**24**]. It is critically important to study and model the creep deformation and damage of 304 SS at high temperature. Moreover, 304 SS does not show an abrupt boundary between elastic and inelastic deformation rather it shows a unified viscoplastic response thus it is susceptible to room temperature creep or relaxation depending on applied boundary conditions [**24**].

Secondary creep based classical life prediction models such as Larson-Miller [**29**], Manson-haferd [20] or Monkman-Grant [**30**] models can only predict the rupture life. Moreover, under high load and high temperature the tertiary creep regime can initiate quickly and unexpectedly where primary and secondary regimes are subordinate [**27**], [**28**]. Models incorporating the tertiary regime are needed. Often the primary creep regime is a short lived phenomenon in creep deformation and can be neglected in gas turbine applications.

Cauvin et. al [**31**] characterized damage in three scales micro-, meso- and macro-scales. Atomic voids and dislocations appear on the micro-scale while visually or near-visually observable damage is in the macro-scale. The meso-scale consists of a representative volume element that averages the effects of micro-scale cracks, voids and other distributed deteriorations. It is the meso scale that should be accounted for when using continuum damage mechanics (CDM).

Marigo [**32**] stated that damage takes place when atomic bonds breaks at microstructural level and damage represents surface discontinuities in the form of micro-cracks and volume discontinuities in the form of cavities. Lindborg [**33**] explained that localized stress concentrations mount up due to micro-cracks which can cause rapid plastic or visco-plastic flow at the crack tips and pointed out that sharp cracks are more critical for damage than round voids. Ibijola [**34**] classified damage as brittle when the crack initiates at the meso scale without plastic

strain and damage is ductile when damage occurs simultaneously with plastic deformation. Lemaitre [**35**] added that cracks and voids inside materials are oriented randomly. Chaboche [**36**] and Cordebois and Sideroff [**37**] considered these orientations as an intrinsic variable of damage. Ibijola [**34**] proposed a model assuming that cracks and voids are equally distributed in all directions inside the material and do not depends on orientation. Raghavan et al [**38**] and Cauvin et al [**31**] considered that there is two complementary approaches to damage, one that focuses on actual damage manifestations at meso scale (the micro-mechanics approach) and the one that assumes homogeneous relation with damage (the phenomenological approach), which has been termed as continuum damage mechanics. Hill [**39**] and Hashin [**40**] have done significant work on micromechanics approach and solved boundary value problem of Representative Value Element (RVE) with microstructure distribution. Kachanov [72] originated the phenomenological CDM field for damage modeling. Rabotnov [**73**] extended the work of Kachanov by incorporating damage into the creep strain rate and related damage as cross-sectional area fraction of cavities for uniaxially stressed specimen which is known as the Kachanov-Rabotnov (KR) damage model. Later this KR model is extensively used in creep damage modeling by Lemaitre and Cahaboch [**41**], Voyiadji's and Kattan [**42**], Oyane [**43**], Rousselier [**44**], and Simo and Ju [**45**]. Later, KR model was further extended by Penny [**49**],[**50**] to extrapolate long rupture time creep behavior using short rupture time creep data, which was tested and analyzed by Furtado et. al **[81]** for reliability. May et al [**82]** analyzed KR model for high temperature and discussed the relation between the damage function and void formation.

The Kachanov-Rabotnov (KR) model has been found to accurately predict creep deformation and has become easier to use since the development of new approaches to determine the materials constants [**28**]; however, the KR model is still limited by the fundamental form of the coupled creep strain and damage evolution equations. The KR approach is considered a local CDM approach where rupture is reached when the damage variable within a representative volume element becomes unity. However, in application it is reported that rupture takes place when analytical damage is well below unity, a result that is unrealistic and against the

assumption of KR approach [**46**],[**50**]. Liu and Murakami [64], Hyde et. al [63], and Wen et al [**57**] have observed the stress sensitivity and mesh dependency of the KR model. Due to stress sensitivity the KR damage rate becomes infinitely large near rupture time, which further contributes to mesh dependency in Finite Element Method (FEM) analysis. Due to mesh dependency FEM analysis exhibits a localized brittle-type damage distribution around the crack tip and does not converges to a unique solution upon mesh element refinement. Thus a improved approach is needed to overcome this stress-sensitivity and to model the damage evolution from zero to unity at rupture. It is hypothesized that this can be done by introducing new coupled creep-damage equations with a better functional form that will always produce critical damage equal to unity at rupture.

Recently, a novel multistage Sinh model has been proposed by Stewart [**5**] that can model primary, secondary and tertiary stages. The Sinh model does not show stress sensitivity and damage does not becomes unreasonable large near rupture time while compared with KR model. Unlike the KR model, with the Sinh model fracture occurs when the damage value becomes unity. In this study, creep tests at four different stress levels and two different temperatures that have been repeated five times (total twenty data sets) are collected from literature [**65**] and are used to compare the KR and Sinh models. Analytical approaches to evaluate the material constants of each model are discussed in detail. The difference between creep strain, damage evolution, and critical damage predictions are discussed. Finally, additional creep rupture data, collected from literature [66[**67**] is used to compare the creep life prediction capability of these two models. It is found that the Sinh model provides a more accurate assessment of the creep damage behavior and better predicts rupture when compared to KR model.

4.1 KACHANOV-RABOTNOV LOCAL APPROACH MODEL

The classical life prediction methods (including Larson-Miller, Monkman Grant etc.) that are used in industry are slowly being replaced by Continuum Damage Mechanics (CDM) based

damage rate equations that can provide accumulated damage, residual life, and rupture life prediction for a given stress. The presence and development of an internal damage/cavity leads to gradual loss of material strength. The main purpose of Continuum Damage Mechanics is to taking this into account. Generally, the damage is considered as continuum (homogeneous throughout a representative volume element) thereby the expression continuum damage mechanics is used.

During the strain process irreversible defects appear due to localization and there occurs a accumulation of dislocations (inter-crystalline cavities in creep, persistent slip band in fatigue etc). These processes are considered damage. Remaining Life has also be used as a metric of damage; where, when the remaining life under a given loading condition is less than the nominal life, damage is in existence [**68**],[**69**]. Generally, creep damage can be classified in two forms: trans-granular (ductile) damage, and inter-granular (brittle) damage. Trans-granular damage arises when slip bands are forming under high stress and low temperature. Inter-granular damage arises when micro-cracking takes place at grain boundaries under high temperature and low stress [**70**],[**71**].

Growth and accumulation of cavities under creep conditions lead to a reduction in the effective cross section and thus an increase in the effective stress. For the calculation of damage, three type of stress can be considered. The first is the true stress which accounts for geometric reduction in cross section due to macroscopic deformation [**68**].

$$\sigma_T = \frac{F}{A} = \sigma \cdot (1 + \varepsilon) \tag{4.1}$$

where σ_T is true stress, F is applied force, A is initial cross-sectional area, σ is engineering stress and ε is engineering strain. The second is net stress which accounts for geometric homogenization

$$\sigma^* = \sigma_T \cdot \left(\frac{A}{A^*} \right) = \frac{\sigma_T}{(1-\Omega)} \tag{4.2}$$

where the present cross-sectional area is equal to $A^* = A \cdot (1-\Omega)$, $A\Omega$ is the mean area of de-cohesion, and Ω is the fraction of area de-cohesion thus the net stress is higher than the true stress. Finally there is effective stress which accounts for local stress concentration, the interaction between defects, and mechanical behavior homogenization. Effective stress can be defined as the stress required to attain macroscopic strain ε on the undamaged volume element subject to the engineering stress σ_E [**68**],[**69**].

$$\begin{aligned} \bar{\sigma} &= \sigma_E \cdot \frac{A}{A_{net}} = \frac{\sigma_E}{(1-D)} \\ D &= 1 - \frac{\bar{E}}{E} \end{aligned} \tag{4.1}$$

where A_{net} is effective area, D is damage, $\bar{E}$ and E are the effective and engineering elastic modulus respectively.

In the Kachanov-Rabotnov model amplified stress due to a local reduction in cross-sectional area is the basis of the damage variable, ω. The reduction in cross section area is due to formation of microcracks, cavities and voids. This reduction in area affects a net increase in stress and thus the effective stress.

$$\bar{\sigma} = \sigma \cdot \frac{A}{A_{net}} = \frac{\sigma}{(1 - \frac{A - A_{net}}{A})} = \frac{\sigma}{(1-\omega)} \tag{4.2}$$

where A is the initial area, A_{net} is the current area, $\bar{\sigma}$ is the effective stress and σ is the equivalent stress. In CDM, damage ω, is assumed to be homogeneous and irreversible. The Kachanov-Rabotnov [72],[**73**] coupled creep-damage constitutive equations are as follows

$$\dot{\varepsilon}_{cr} = \frac{d\varepsilon_{cr}}{dt} = A \cdot (\frac{\sigma}{1-\omega})^n \tag{4.5}$$

$$\dot{\omega} = \frac{d\omega}{dt} = \frac{M \cdot \sigma^x}{(1-\omega)^\phi} \tag{4.6}$$

where A and n are the Norton power law constants, σ is equivalent stress and M, χ and ϕ are tertiary creep damage constants. The χ constant controls the magnitude of M and can be set arbitrarily to any number greater than or equal to unity. Rupture time and critical damage can be predicted by integration of the damage evolution [Eq.(4.6)] and assuming initial time t_0 and initial damage ω_0 is equal to zero [**74**].

$$t = [1-(1-\omega)^{\phi+1}] \cdot [(\phi+1) \cdot M \cdot \sigma^x]^{-1} \tag{4.7}$$

$$\omega(t) = 1-[1-(\phi+1) \cdot \mathrm{M} \cdot \sigma^x \cdot t]^{\frac{1}{(\phi+1)}} \tag{4.8}$$

The tertiary creep constant M can be calculated by rearranging [Eq. (4.8)]

$$M = \frac{1-(1-\omega_r)^{\phi+1}}{(\phi+1) \cdot \sigma^x \cdot t_r} \tag{4.9}$$

At rupture time, assuming the rupture damage $\omega_r = 1$ gives

$$M = \frac{1}{(\phi+1) \cdot \sigma^x \cdot t_r} \tag{4.10}$$

In 1967, Kachanov [72] observed a varying creep ductility but did not identified the damage mechanism responsible for tertiary creep. Kachanov assumed creep displacement rates are much faster within the uncavitated regions than cavity growth regions and cavitation does not affect the macroscopic creep deformation. Fracture occurs when cavities are linked up throughout whole transverse grain boundaries. He was wrong. This initial model did not predict tertiary creep for constant stress conditions. Later, in 1969, Rabotnov [73] assumed the creep displacement rates is slower at the uncavitated regions than those of cavity growth regions. Thus, stress is loaded up to

the uncavitated zones from fast growing cavitated zones that increases the creep rate by reducing the creep controlling effective stress. Rabotnov coupled the damage with the creep rate through an stress increment associated with a load reduction in bearing area as the cavitations/damage develops. This coupled model leads to an accelerated/tertiary creep rate [38].

One of the major drawback of KR model is the difficulty determining the tertiary creep damage constants which has been solved by Stewart et. al [**69**] where two analytical approach (Strain approach and Damage approach) were developed. In the strain approach (SA) the damage evolution equation is incorporated into the creep strain rate equation. In the damage approach (DA) creep strain data is used to approximate damage evolution. For brevity the detailed derivation and discussion of the approaches are not covered here.

4.1.1 Strain Approach

In the Strain Approach (SA) the damage prediction equation, [Eq. 4.8] is introduced into the creep strain rate [Eq.(4.5)] and integration is performed to get a creep strain equation. Then the M constraint [Eq.(4.9)], is introduced and the equation simplified to produce the following creep strain formulation

$$\varepsilon_{cr}(t) = \frac{A \cdot (\phi + 1) \cdot [t \cdot \left(\frac{\sigma}{\tau}\right)^n - t_r \cdot \left(\frac{\sigma}{\tau}\right)^n + t_r \cdot \sigma^n]}{1 + \phi - n}, \tau = \left(1 - \frac{t}{t_r}\right)^{\frac{1}{1+\phi}} \tag{4.11}$$

here, both the *M* and χ tertiary creep damage constants are eliminated. The χ constant can be set arbitrarily to any number greater than or equal unity. The *M* constant should be calculated from [Eq.(4.9)]. The constant, ϕ , can be determined from available creep strain data using the modified creep strain equation, [Eq.(4.11)] and regression software.

4.1.2 Damage Approach

In the Damage Approach (DA), the creep strain rate equation, [Eq.(4.5)] is algebraically rearranged to get analytical damage at each time step

$$\omega\left(\dot{\varepsilon}_{cr}\right)=\frac{\left(\frac{\dot{\varepsilon}_{cr}}{A}\right)^{1/n}-\sigma}{\left(\frac{\dot{\varepsilon}_{cr}}{A}\right)^{1/n}} \tag{4.12}$$

Thus the creep strain rate from experiments ($\dot{\varepsilon}_{cr}$) will produce an analytic damage curve, $\omega(\dot{\varepsilon}_{cr})$. The introduction of *M* constraint [Eq. (4.9)] into the damage prediction equation [Eq. (4.8)] gives the following

$$\omega(t)=1-\left[\frac{t}{t_r}\cdot[(1-\omega_r)^{\phi+1}-1]+1\right]^{\frac{1}{\phi+1}} \tag{4.13}$$

where the tertiary creep damage constant, ϕ , is the only unknown. The constant ϕ can be determined by using the available creep strain data, the analytic damage equation, [Eq. 4.8], the modified damage equation, [Eq. 4.13], and regression analysis software. . The χ constant can be set arbitrarily to any number greater than or equal unity. The *M* constant should be calculated from [Eq. (4.9)].

4.1.3 Limitations of Local Approach

Damage at Rupture is not Unity

Rearranging strain rate [Eq. (4.5)] we get

$$\omega\left(\dot{\varepsilon}_{cr}\right)=\frac{\left(\frac{\dot{\varepsilon}_{cr}}{A}\right)^{1/n}-\sigma}{\left(\frac{\dot{\varepsilon}_{cr}}{A}\right)^{1/n}} \tag{4.14}$$

When $\dot{\varepsilon}_{cr}=\dot{\varepsilon}_{cr_{\min}}$ the denominator of [Eq. 4.14] takes the form of Norton Power law, and is equal to equivalent stress σ. The ratio of [Eq. (4.14)] becomes unity and the damage becomes zero. As soon as $\dot{\varepsilon}_{cr}>\dot{\varepsilon}_{cr_{\min}}$, the term $\left(\dot{\varepsilon}_{cr}/A\right)^{1/n}$ represents instantaneous effective stress, higher than equivalent stress (σ), and irreversible damage starts to grow. Thus, in KR model damage builds up only in tertiary creep stage, no damage accumulates in primary and secondary creep stages. For damage to be unity at failure, instantaneous strain ($\dot{\varepsilon}_{cr}$) has to be infinitely large. But

creep strain rate becomes large just before failure and remains finite throughout the lifetime. Thus, KR model damage remains very low up to 90% of lifetime. Moreover, $\dot{\varepsilon}_{cr}$ is never infinitely large thus damage cannot be unity and varies from 0.2-0.8 for most metals [**38**]. This can also be realized from damage rate [Eq. (4.6)]. When damage approaches to unity, damage rate becomes infinitely large suggesting that the function attempts to encapsulate both the continuous damage of creep and discontinuous plastic damage that occurs at the instant of fracture [**38**]. A better approach is needed to overcome this issue.

Integrating damage evolution [Eq. 4.6] and assuming initial time t_0 and initial damage ω_0. is equal to zero giving

$$\omega(t) = 1 - [1 - (\phi + 1) \cdot \mathrm{M} \cdot \sigma^{x} \cdot t]^{\frac{1}{(\phi+1)}} \tag{4.15}$$

At time $t = t_r$,damage $\omega = \omega_r$, rearranging [Eq. (4.15)] becomes

$$M = (1 - (1 - \omega_r)^{(\phi+1)}) / ((\phi + 1)\sigma^{\chi} t_r) \tag{4.16}$$

Introducing [Eq. (4.16)] into [Eq. (4.15)] gives the following

$$\omega(t) = 1 - \left[\frac{t}{t_r} \cdot [(1 - \omega_r)^{\phi+1} - 1] + 1 \right]^{\frac{1}{\phi+1}} \tag{4.17}$$

If it is assumed that at failure $\omega_r = 1$, equation (4.17) reduces to

$$\omega(t) = 1 - \left(1 - \frac{t}{t_r} \right)^{\frac{1}{\phi+1}}, (\phi > 1) \tag{4.18}$$

In this form KR damage only depends on ϕ value. Figure 4.1 (a) shows that theoretically critical damage at failure can be unity in the form of [Eq. (4.18)] and exhibits stress sensitivity as discussed in introduction section. Problem arises during implementing the KR model on experimental data; critical damage have to be determined from [Eq. (4.14)], which cannot be unity $(\omega(\dot{\varepsilon}_r) \neq 1)$. Thus the KR model damage-trajectory governing equation does not reduces to

[Eq. (4.18)] and unable to reach unity at failure and violets the presumption of unity critical damage at rupture.

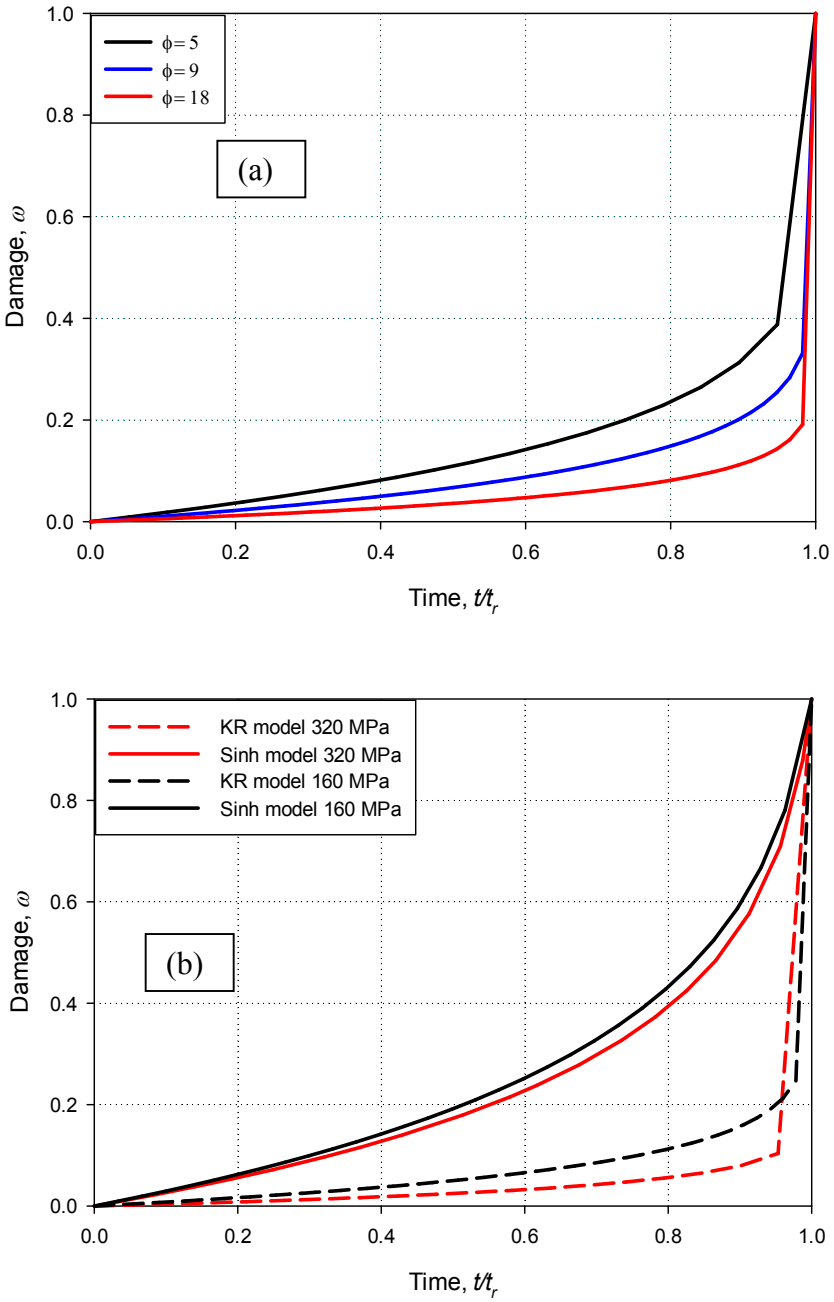

Figure 4.1: (a) Normalized time vs Damage. Typical KR damage evolution at different ϕ, (b) Comparison of typical KR and Sinh model

Stress sensitivity

Kachanov-Rabotnov's (KR) local CDM approach model shows stress sensitivity. In the KR approach damage is assumed to be an internal state variable which evolves from zero to critical damage of fracture, $(0 \le \omega < \omega_{cr})$, where critical damage is often assumed equal to unity $(\omega_{cr} = 1)$. Qi et al. [**46**] and Lemaitre [**47**] made it clear that the assumption that critical damage is equal to unity is not realistic. The value of critical damage is less than unity and varies from 0.2-0.8 for most metals. Chaboche [**48**], explained that, KR model uses local cross-sectional area reduction to account for effective stress amplification during damage [Eq. (4.15)], but in reality microscopic damage gives little loss of effective area before crack initiation thus the damage variable (ω) is a very small value until a large fraction of life has been exhausted. He proposed that an improvement can be obtained by introducing an additional damage parameter. The KR model tries to model both the creep damage and instantaneous plastic damage to rupture within a continuous function; however, the very high rate of damage that occurs during instantaneous plastic damage cannot be accommodated, thus the KR model develops critical damage values equal to much less than unity. Penny [**49**] stated that the damage rates of KR model become excessively high at about 90% of lifetime such that the critical damage ω_{cr} cannot be unity. This becomes readily apparent by examining the damage function of KR [Eq. (4.16) and (4.17)], as follows

$$\dot{\varepsilon}_{cr} = f\left(\frac{1}{(1-\omega)^{n}}\right) g\left(\sigma, \mathrm{T}\right) \tag{4.19}$$

$$\dot{\omega} = f\left(\frac{1}{(1-\omega)^{\phi}}\right) g(\sigma, \mathrm{T}) \tag{4.20}$$

when, damage approaches unity these functions becomes infinitely large suggesting that these functions attempt to encapsulate both the continuous damage of creep and the discontinuous plastic damage that occurs at the instant of fracture [**51**]. For further proof of this problem, taking the variation of damage $\partial\omega(t)$, [Eq. (4.15)], with an infinitesimal variation of stress $\partial\sigma(t)$ produces

$$\partial\omega(t) = \chi \frac{M \cdot \sigma(t)^{\chi} \cdot t}{[1-(\phi+1)\cdot M \cdot \sigma(t)^{\chi} \cdot t]^{\frac{\phi}{\phi+1}}} \cdot \frac{\partial\sigma(t)}{\sigma(t)} \tag{4.21}$$

Replacing the portion, $M \cdot \sigma(t)^{\chi} \cdot t$, by rearranging [Eq.(4.15)] and introducing into the above equation provides

$$\partial\omega(t) = \chi \cdot \frac{1-(1-\omega)^{\phi+1}}{(1-\omega)^{\phi}} \cdot \frac{\partial\sigma(t)}{\sigma(t)} \tag{4.22}$$

when damage is critical $(\omega_{cr} \to 1)$, the damage variation $\partial\omega(t)$ is near infinite as the denominator becomes zero thus damage cannot be equal to unity. To overcome these issues a damage evolution equation which exhibits a finite variation of damage $\partial\omega(t)$ under an infinitesimal variation of stress $\partial\sigma(t)$ should be developed.

Murakami and Liu [**51**],[**52**], Bazant [**53**], Jian et al. [**57**], Ladevege [**54**], and Hyde [**58**] have written papers describe the limitations of the local CDM approach. These authors observed damage localization around the crack tip in FEM analysis and experienced mesh dependency where the FE solutions upon mesh refinement do not converge to a single solution. Mesh dependency analysis is covered in FEM analysis chapter.

4.2 NOVEL SINH (SIN HYPERBOLIC) MODEL

In this study, a CDM-based Sinh creep damage constitutive model is used. A detail monograph is stated in Stewart [**5**]. Classically, the simplest stage of creep to analysis is the secondary stage where a balance between hardening and recovery mechanisms leads to a steady-state/minimum creep strain rate, $\dot{\varepsilon}_{\min}$. This secondary viscous function must be found first. Among the most common forms of secondary creep modeling it is reported that the equation developed by Mcvetty [**55**] has the highest quality fit [**5**] where A (1/s) and σ_s (MPa) are the creep coefficient and secondary creep mechanism-transition stress respectively.

$$\dot{\varepsilon}_c = A \sinh\left(\sigma/\sigma_s\right) \tag{4.23}$$

4.2.1 Creep Strain Rate and Analytical Damage

The CDM based damage variable has three functions; to model the tertiary creep regime, track the evolution of creep damage & predict rupture. To achieve these goals the damage variable, ω , is coupled to the secondary viscous function as follows

$$\dot{\varepsilon}_{sc} = f(\sigma)\cdot g(T)\cdot h(\omega) \tag{4.24}$$

where the $h(\omega)$ function describes how the current state of damage influences the strain rate. A detail monograph of the damage evolution is derived in the Stewart PhD dissertation work [**5**]. Introducing $h(\omega)$, into the total creep strain rate, $\dot{\varepsilon}_{cr}$,[Eq.(4.23)],and solving for $h(\omega)$ produces

$$h\left[\omega(t)\right] = \frac{\dot{\varepsilon}_{cr}(t)}{A\sinh\left(\sigma/\sigma_s\right)} \tag{4.25}$$

It is proposed that $h(\omega) = \exp(\lambda\omega^p)$, where λ and p are unit-less material constants. Introducing it into above equation and solving for damage provides

$$\omega^*(t) = \left\{\frac{1}{\lambda}\ln\left[\frac{\dot{\varepsilon}_{cr}(t)}{A\sinh\left(\sigma/\sigma_s\right)}\right]\right\}^{1/p} \tag{4.26}$$

where $\omega^*(t)$ is the analytical damage derived from the creep strain rate, $\dot{\varepsilon}_{cr}(t)$. Considering the time just before fracture $t \simeq t_r$, where $\dot{\omega}_{cr} = 1$, the creep strain rate, [Eq. (4.25)], becomes

$$\begin{aligned} &\dot{\varepsilon}_{cr} = \dot{\varepsilon}_{final} \approx A\sinh\left(\sigma/\sigma_s\right)\exp(\lambda) \\ &\lambda = \ln\left(\frac{\dot{\varepsilon}_{final}}{\dot{\varepsilon}_{\min}}\right); \qquad \dot{\varepsilon}_{\min} = A\sinh\left(\sigma/\sigma_s\right) \end{aligned} \tag{4.27}$$

where the material constant λ can be determined from experimental data. It is proposed that the best value for *p* is 3/2 unit-less. Thus, the creep strain rate of the sinh model becomes,

$$\dot{\varepsilon}_{cr} = A\sinh\left(\sigma/\sigma_s\right)\exp\left(\lambda\omega^{3/2}\right) \tag{4.28}$$

4.2.2 Damage Model

Using the concept of Liu and Murakami [64], that the problem of stress-sensitivity and mesh-dependence can be mitigated by representing damage as an exponential function within the creep rate and damage evolution equations, the following damage evolution equation is proposed

$$\dot{\omega} = \frac{M\left[1-\exp(-\phi)\right]}{\phi}\sinh\left(\frac{\sigma}{\sigma_t}\right)^{\chi}\exp(\phi\omega) \tag{4.29}$$

where M, ϕ, χ, and σ_t are material constants that must be greater than zero. The portion $\left[1-\exp(-\phi)\right]/\phi$ is necessary to avoid an undefined error when the damage evolution equation is integrated. Integration of [Eq. (4.29)] with the assumption of initial time, t_o and initial damage, ω_o equals to zero, gives the following damage and rupture prediction equation

$$\omega(t) = -\frac{1}{\phi}\ln\left[1-\left[1-\exp(-\phi)\right]\frac{t}{t_r}\right]; \qquad t_r = \left[M\sinh\left(\frac{\sigma}{\sigma_t}\right)^{\chi}\right]^{-1} \tag{4.30}$$

The constants M, χ, & σ_τ can be found using stress-rupture data. The remaining constants ϕ, can be determined simultaneous by minimizing the error of the following equation [combination of Eqs. (4.26) & (4.30)]

$$\begin{aligned} &\omega(t) = \omega^*(t) \\ &-\frac{1}{\phi}\ln\left[1-\left[1-\exp(-\phi)\right]\frac{t}{t_r}\right] = \left\{\frac{1}{\lambda}\ln\left[\frac{\dot{\varepsilon}_{cr}(t)}{A\sinh(\sigma/\sigma_s)}\right]\right\}^{1/p} \end{aligned} \tag{4.31}$$

Chapter 5: Numerical Results

Experimental data collected from literature [**65**] for 304 STS at four stress levels (160, 180, 300,320 MPa) and two temperatures (600-700°C) is used. For repeatability, each test type is repeated five times, thus a scatter band and a probable deviation can be observed.

5.1 KACHANOV RABOTNOV MODEL:

A list of optimized constants for the KR model is presented in Table.

Table 5.1: Kachanov-Rabotnov material constants for 304 SS

Test	Temp, T ($°C$)	Stress, σ (MPa)	A (MPa^{-n} hr^{-1})	n	Strain Approach			Damage Approach		
					M ($MPa^{-\chi}$ hr^{-1})	χ	ϕ	M ($MPa^{-\chi}$ hr^{-1})	χ	ϕ
1	700	160	6.53E-31	12.78	1.01E-10	3	12	9.71E-11	3	12.5
2	700	180	6.53E-31	12.78	1.0E-10	3	18	9.80E-11	3	18.5
3	600	300	1.56E-35	13.36	1.05E-11	3	27	7.56E-12	3	38
4	600	320	1.56E-35	13.36	2.22E-11	3	24	1.97E-11	3	27

The creep strain of the tests performed at 700°C, and 160 MPa and 180 MPa respectively are plotted in response to the KR model in Figure 5.1 (a). The creep strain of the test performed at 600°C, and 300 MPa and 320 MPa respectively are plotted in response to the KR model (both SA and DA approach) in Figure 5.1 (a). In Figure and Figure it is evident that the model goes through the middle of the scatter band. The material constants were obtained by fitting to the repeat test nearest the middle of the scatter band. Values of constant A and n were evaluated using Norton power law ($\dot{\varepsilon}_{\min} = A \bullet \sigma^n$). Next, the values of A were fitted to a exponential equation ($A(T) = B\exp(-Q/RT)$) for temperature dependence where the pre-exponent factor constant B and Q are optimized to $1.45\times10^{10}\,MPa^{-1}hr^{-1}$ and $751.5 Jmol^{-1}$ respectively. A temperature-dependant function for $n(T)$ is required. Using Eureqa optimization software, [**19**] a

linear equation in found to generate straight line dependence over temperature which gives $n = 18.42 - 0.0058 * T$ with a goodness of fit of $R^2 = 0.98$. The remaining constants M, χ ,and ϕ were found using the Strain (SA) and Damage (DA) approaches. For the strain approach (SA) the experimental creep data was fit to the strain [Eq.(4.11)] and optimized values of M, χ ,and ϕ obtained [see Table 5.1], These constants were plugged into [Eq. (4.13)] to evaluate damage evolution using SA. For the Damage Approach (DA), analytical damage is calculated using [Eq. (4.12)] then M, χ ,and ϕ constants were optimized through comparing with the damage prediction [Eq. (4.17)]. These constants are used in [Eq. (4.11)] to evaluate the creep strain using DA. Plots of the Kachanov-Rabotnov damage model fit to analytical damage data [Eq. (4.12)] are shown in Figure 5.3 and Figure 5.4 (a). Examining Figure 5.1 to 5.4 is observed that both the strain and damage approach to constant determination for the KR model can model the creep deformation and damage of 304 SS.

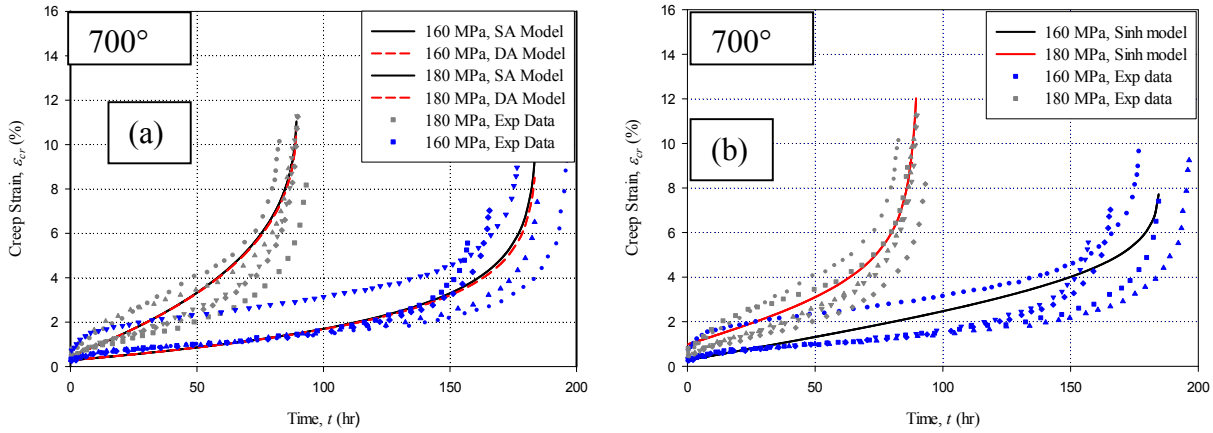

Figure 5.1: Creep deformation simulation at 700°C, (a) Kachanov-Rabotnov and (b) Sinh model

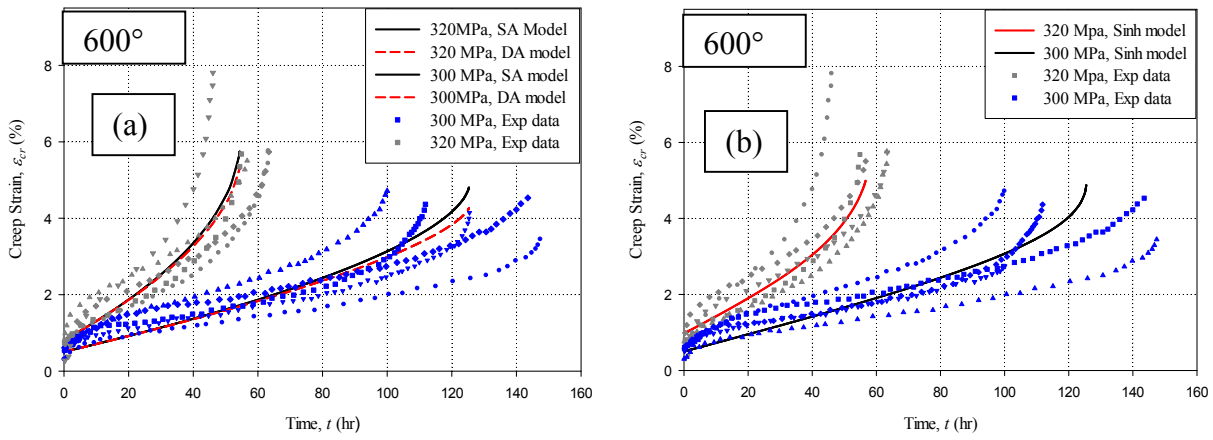

Figure 5.2: Creep deformation simulations at 600°C, (a) Kachanov-Rabotnov and (b) Sinh model

5.2 NOVEL SINH MODEL

The same experimental data sets are used to determine the material constants of the Sinh model. The secondary creep constants A and σ_s are determined from minimum creep rate and model equation [Eq. (4.27)]. The unit-less material constant λ are found for each data set using [Eq. (4.27)]. The value of ϕ is determined by minimizing the error of [Eq. (4.31)]. A list of the optimized constants for the sinh model are presented Table 5.2.

Table 5.2: Sinh model material constant for 304 SS

Test	Temp., T (°C)	Stress, σ (MPa)	A (%hr^{-1})	σ_s (MPa)	λ	ϕ	χ	M hr^{-1}	σ_t (MPa)
1	700	160	1.48E-4	27.99	4.517	5.5	3	0.024	289.44
2	700	180	1.48E-4	27.99	4.24	3.8	3	0.028	289.44
3	600	300	1.45E-6	24.76	3.72	5.99	3	0.003	257.08
4	600	320	1.45E-6	24.76	1.93	2.62	3	0.004	257.08

The constant λ is the natural logarithm of the quotient of final and minimum strain rate. As creep strain rate depends on stress and temperature, the λ constant also evolves accordingly. From Table 5.2 it is observed that with a decrease in stress the constant λ increases. At lower stress, machine components deforms slowly towards failure causing a lower $\dot{\varepsilon}_{\min}$ value, thus λ increases. Not enough experimental data is available about thefinal creep strain rate $\dot{\varepsilon}_{final}$ to generalize these statement across all levels of temperature & stress.

The constant ϕ controls the trajectory of the Sinh damage model curve. At $\phi = 1$ the curve becomes a straight-line from zero to unity. For a given temperature, the value of ϕ increases with decreasing stress. At low stress, machine components have comparatively higher life. The damage evolution must have a long trajectory path to accommodate longer life. Increasing the value of ϕ accommodates such a cover. Thus the constant ϕ guides the damage model trajectory.

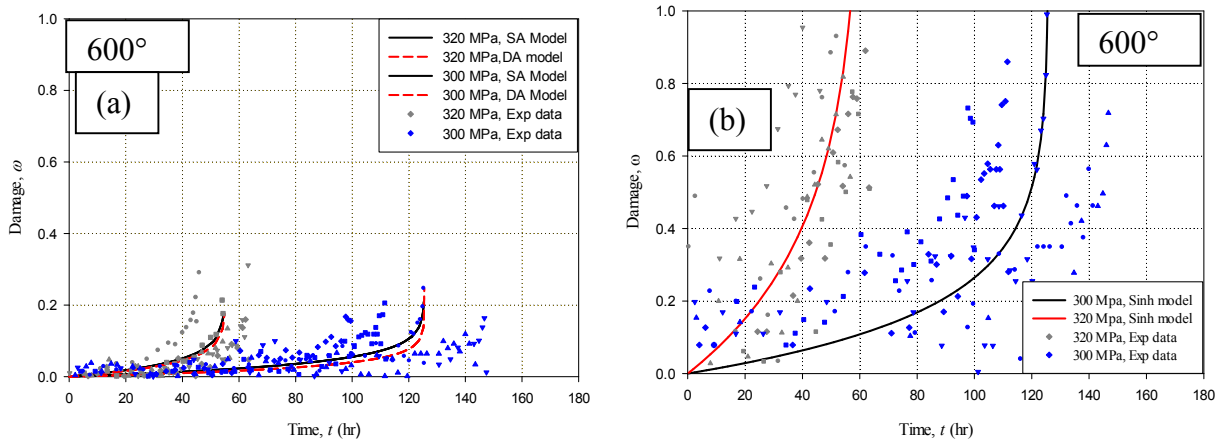

Figure 5.3: Damage evolution simulations at 600°C, (a) Kachanov-Rabotnov and (b) Sinh model

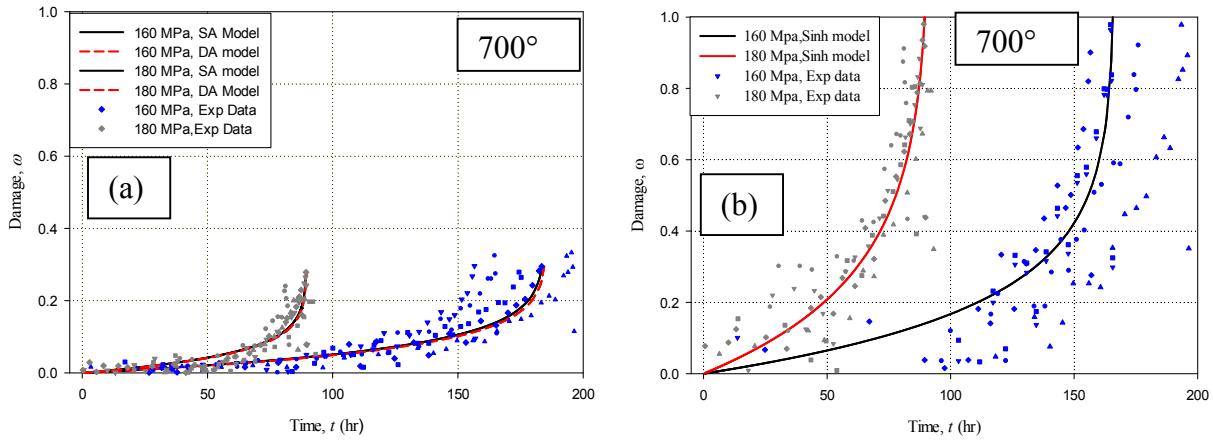

Figure 5.4: Damage evolution simulationat 700°C, (a) Kachanov-Rabotnov and (b) Sinh model

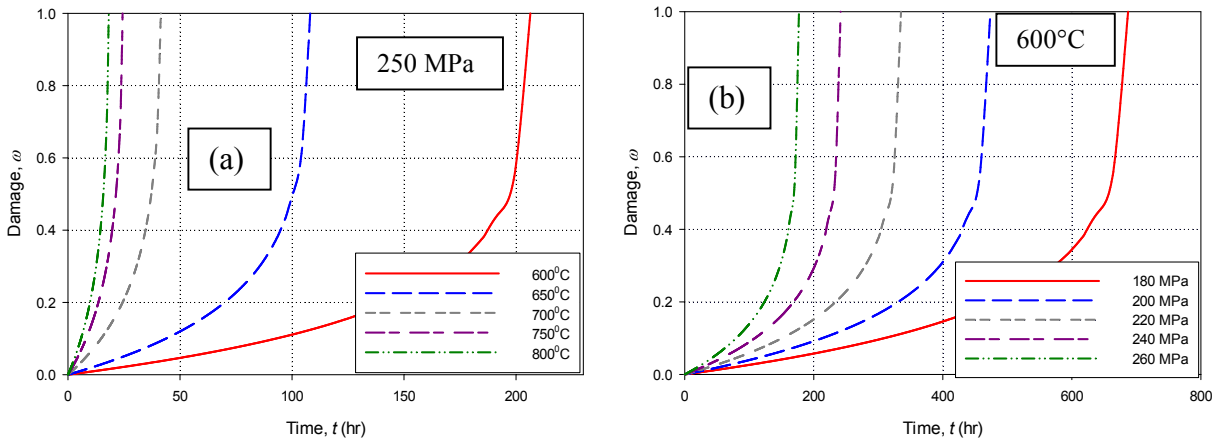

Figure 5.5: Parametric simulation of Sinh damage evolution curve (a) at varying temperature and constant stress (b) at varying stress and constant temperature

Figure 5.5 (a) shows the nature of the Sinh damage model at constant stress and varying temperature. The constants M, σ_t and ϕ are temperature dependent such that a change in temperature will produce a different damage history. The higher the operating temperature the shorter the creep life. The predicted rupture life (t_r) is determined first [Eq. 4.30]. Constant $M(T)$ and $\sigma_t(T)$ accommodate the temperature-dependent of creep life. Next, the predicted rupture life (t_r) is introduced into the damage curve ω [Eq. 4.30]. Thus for each and every simulation, the critical damage is unity.

Figure 5.5 (b) shows the nature of the Sinh model at constant temperature for varying stresses. The constant ϕ is temperature dependent and controls the curvature of the damage curve. The $\phi(T)$, $M(T)$, and $\sigma_t(T)$ are constants carry temperature dependence. The predicted rupture life accommodates the effect of different stress level [Eq. 4.30] on creep life. The damage curve varies with different predicted rupture life.

5.2.1 Advantage of Sin-hyperbolic model

Constitutive creep damage evolution Sinh models are written as follows [**74**]

$$\dot{\varepsilon}_{cr} = A\sinh\left(\sigma/\sigma_s\right)\exp\left(\lambda\omega^{3/2}\right) \tag{5.1}$$

$$\dot{\omega} = \frac{M\left[1-\exp\left(-\phi\right)\right]}{\phi}\sinh\left(\frac{\sigma}{\sigma_t}\right)^{\chi}\exp\left(\phi\omega\right) \tag{5.2}$$

where A (1/s) and σ_s (MPa) are the creep coefficient and secondary creep mechanism-transition stress respectively. Determined using Mcvetty minimum creep rate law ($\dot{\varepsilon}_c = A\sinh\left(\sigma/\sigma_s\right)$)from experimental data. λ is unit-less material constants, defined as $\lambda = \ln\left(\frac{\dot{\varepsilon}_{final}}{\dot{\varepsilon}_{\min}}\right)$, can be calculated directly from experimental data. And ω represents damage evolves zero to unity. In damage rate equation M, ϕ , χ , and σ_t are material constants which must be greater than zero.

Rearranging strain rate [Eq. 5.1] giving

$$\omega(\dot{\varepsilon}) = \left\{\frac{1}{\lambda}\ln\left[\frac{\dot{\varepsilon}_{cr}(t)}{A\sinh\left(\sigma/\sigma_s\right)}\right]\right\}^{2/3} \tag{5.3}$$

the term in denominator ($A\sinh\left(\sigma/\sigma_s\right)$) represents minimum creep strain rate (Mcvetty law [**55**]). Damage begins to accumulate when $\dot{\varepsilon}_{cr} > \dot{\varepsilon}_{cr_{\min}}$. Damage is zero when $\dot{\varepsilon}_{cr} = \dot{\varepsilon}_{cr_{\min}}$ and damage is unity when $\dot{\varepsilon}_{cr} = \dot{\varepsilon}_{final}$. The constant λ accommodates this behavior. When $\dot{\varepsilon}_{cr} = \dot{\varepsilon}_{final}$, [Eq. 5.3] is reduced to $\omega(\dot{\varepsilon}_{final}) = \left(\frac{1}{\lambda}*\lambda\right)^{2/3} = 1$. Thus, for each and every experimental data sets the critical

damage is unity at failure. Integrating damage rate [Eq. (5.2)] with the assumption of initial time, t_0 and initial damage ω_0 equal to zero, and solving for damage (ω) giving

$$\omega(t) = -\frac{1}{\phi}\ln\left[1-\left[1-\exp(-\phi)\right]\frac{t}{t_r}\right];$$
$$t_r = \left[M\sinh\left(\frac{\sigma}{\sigma_t}\right)^{\chi}\right]^{-1} \tag{5.4}$$

Taking variation of damage $\partial\omega(t)$ with an infinitesimal variation of stress $\partial\sigma(t)$ giving

$$\partial\omega(t) = \frac{\chi}{\phi}\frac{[1-\exp(-\phi)](t/t_r)}{1-[1-\exp(-\phi)](t/t_r)}\frac{\cosh(\sigma/\sigma_t)}{\sinh(\sigma/\sigma_t)}\frac{\partial\sigma(t)}{\sigma_t} \tag{5.5}$$

No damage term is existing in this [Eq. (5.5)], therefore throughout the damage evolution from zero to unity, $\partial\omega(t)$ remains undisturbed. $\partial\omega(t)$ can be infinite when $t \to t_r$ and denominator term $\left(1-[1-\exp(-\phi)](t/t_r)\right) = 0$. For this to take place, $\exp(-\phi)$ has to be equal to zero at $t = t_r$, and ϕ has to be very large or infinite. But constant ϕ is optimized using equation (5.1) and (5.4). Due to the combined nature of these two equation, with the increase of ϕ , $\dot{\varepsilon}(t)\,\&\,\omega(t)$ for each time step goes down. When ϕ value goes down, $\dot{\varepsilon}(t)\,\&\,\omega(t)$ values goes up. Experimental data fitting using this two equation does not let the ϕ constant to be large value. The maximum value of ϕ to fit experimental data sets ranging from 160Mpa to 320 Mpa and 600°C to 700°C reported is 5.99 [**74**].

For further understanding the issue of analytical critical damage not becoming unity for KR model, experimental data are used to compare the analytical critical damage of these two model. Kim 2007 [**65**] observed natural variation in experimental results under same testing environment. Critical creep strain rate and rupture time varies between experiments of same batch material. Five sets of experiments for each of six different stress level at three different temperature environment has been reported for 304 SS [**65**].

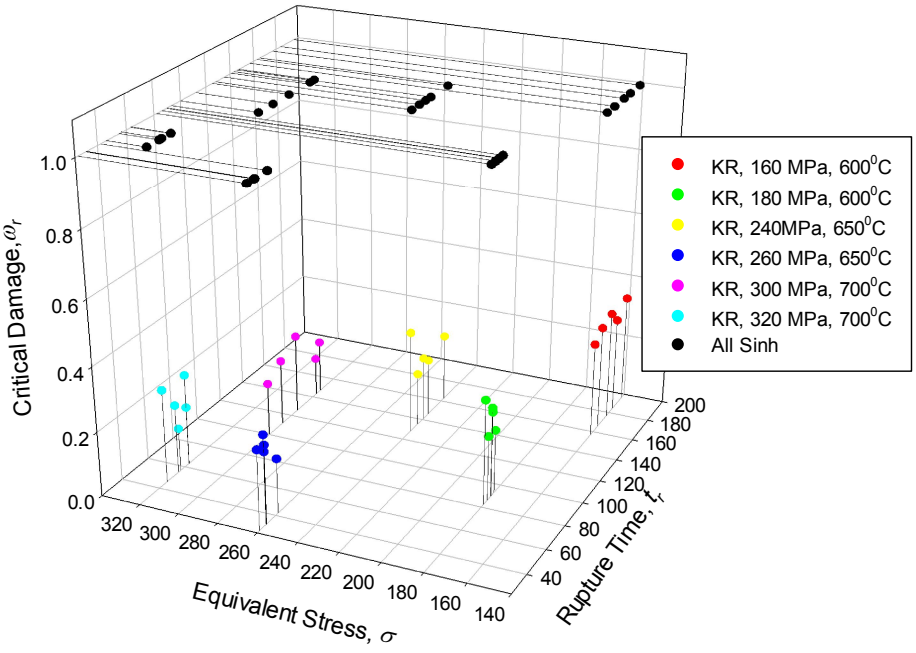

Figure 1.6: Comparison of analytical critical damage of Sinh and KR model

Rearranged strain rate equation of KR and Sinh model [Eq. 4.6 & 4.18] are used to determine critical damage for each of the thirty experiment. Figure 5.6 illustrates the comparison between analytical critical damage of KR and Sinh model. It is evident that sinh model critical damage is always unity while KR model critical damage is less than 0.4 for all tests. Sinh model [Eq. 4.18] normalizes the experimental data and critical damage is always unity at rupture.

5.3 COMPARISON

The ability to accurately model the tertiary creep regime depends on the ability of the secondary viscous function to model the minimum creep rate. The tertiary creep regime arises out of the coupled relationship between the creep strain rate and damage equations. The error observed in modeling the secondary creep regime will persist and increase when attempting to model the tertiary creep regime. The KR model uses the classic Norton Power law to model the minimum creep rate while the Sinh model uses the Mcvetty Sin-hyperbolic law. The sinh model has a

higher R^2 fit to the minimum creep strain rate and thus better models the secondary creep regime. A comparison of experimental minimum creep strain rate with Norton Power and Mcvetty Sinh law is stated in Table 5.3. The Mcvetty model prediction has a cumulative error $\left(\sum abs(actual - predicted)\right)$ of 0.005 while the Norton model prediction has a cumulative error of 0.02. In Figure and Figure 5.1 it is evident that the creep deformation using the KR model damage approach has a closer fit to the Sinh model than the KR model strain approach because the constant determination process for the Sinh model [Eq. (4.28)] explicitly includes damage ω similar to the damage approach of the KR model [Eq. (4.13)].

The damage evolution of both the KR and Sinh model are plotted with experimental (analytically derived) data in Figure 5.3 and Figure 5.4. For the KR model the experimental (analytically determined) damage can have negative values of damage before the minimum creep strain rate is reached. This is because first term of the numerator $\left(\dot{\varepsilon} / A\right)^{1/n}$ for KR analytically derived damage [Eq. (4.6)] yields a stress value that is less than the effective stress σ when the magnitude of the creep strain rate is less than the minimum creep strain rate. The numerator of the analytically derived damage [Eq. (4.12)] becomes negative and thus produces very small negative damage values. These anomalous data points occur during the short primary regime of the creep curve and in the secondary creep regime when extensometer fluctuation cause the creep strain rate to registered as slightly lower than the average minimum creep strain rate. These type of analogous damage data can be neglected. This proves that the KR model generates acceptable analytical damage for the tertiary creep regime.

Table 5.3: Comparison of Norton law and Mcvetty steady-state/minimum creep rate model

Test	Temp. (°C)	Stress (MPa)	Experimental Min. creep strain rate ε(%)	Norton Law	Mcvetty
				KR Model ε(%)	Sinh model ε(%)
1	700	160	0.015949	0.009877012	0.020327856
2	700	180	0.041533	0.04452568	0.041532848
3	650	260	0.107841	0.118131216	0.107634673
4	600	300	0.021393	0.019964073	0.021147343
5	600	320	0.047225	0.047299117	0.047430654
	Cumulative error from Experimental data			0.020856	0.005036777

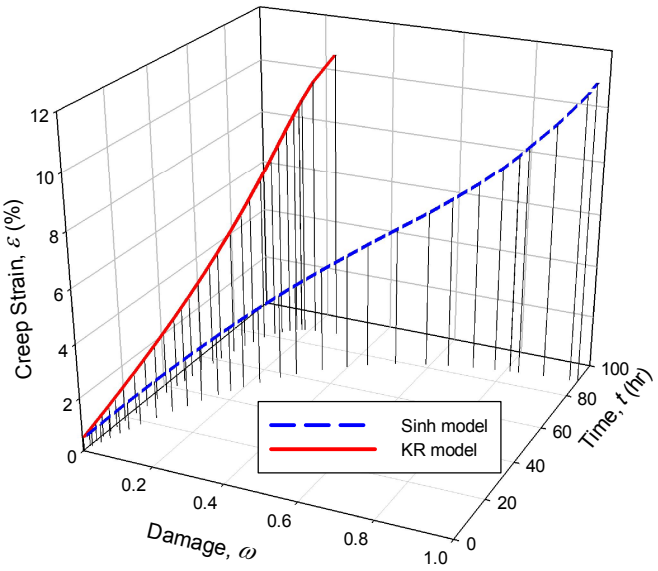

Figure 5.7: 3D trajectory comparison of creep strain and accumulated damage of Sinh and KR model at 180 MPa and 700°C

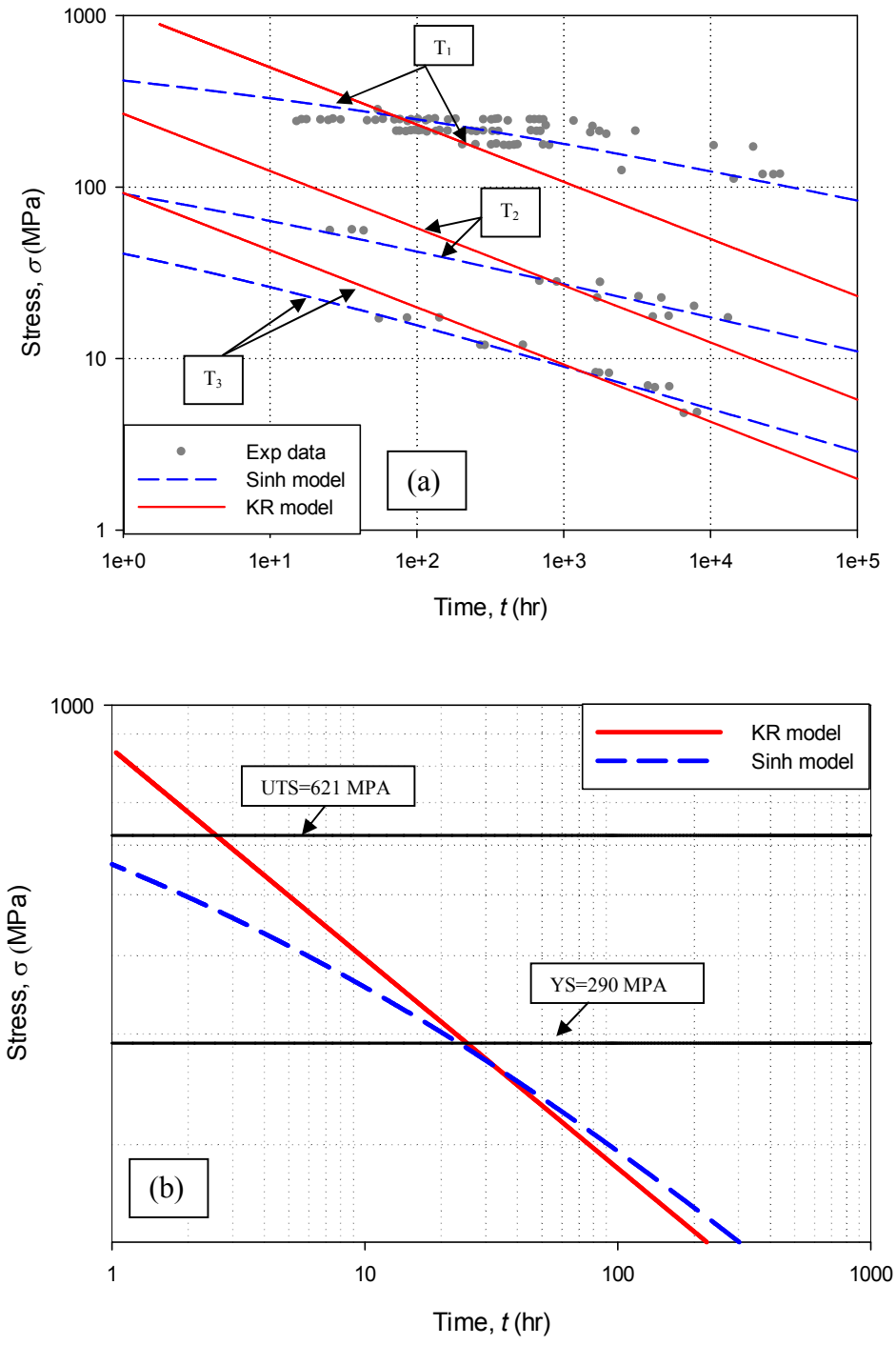

Figure 5.8: (a) Stress vs Rupture time comparison of Sinh and KR model at T_1 =593°C,T_2 =843°C, & T_3 =954°C (b) Characteristics comparison of KR and Sinh model at 700°C.

For Sinh model, the denominator of the analytically determined damage [Eq. (4.26)] is equal to the minimum creep rate for the applied stress. If the creep strain rate is equal to or less than the minimum creep rate, the natural logarithm operator will generate zero or a negative value for the analytical damage. Thus these type of damage are excluded. This proves that the Sinh model generates acceptable analytical damage for the tertiary creep regime.

In terms of easiness to handle, it is easier to find the Sinh model constants as the KR model requires one additional constant than compared to Sinh. In the Sinh model, constants A and σ_s are both dependent on temperature. The constant λ can be directly calculated from experimental data and does not depend on any other constants thus no optimization is needed. The only remaining constant ϕ can be determined from [Eq. (4.31)].

It is ease to determine the Sinh constants. Less constant determination reduces the cumulative error of optimization of curve fitting. In the KR model the constants A and n are both dependent on temperature. Due to the form of the KR damage model, the constant M [Eq. (4.9)] depends on the constant ϕ and the critical damage ω_{cr} (cannot be found directly from experimental data, has to evaluate from [Eq. (4.31)] at the highest creep rate) making it very difficult to optimize.

In damage prediction the Sinh model has a huge advantage as the damage evolution is normalized by the predicted rupture life [t_r, Eq. (4.30)]; thus critical damage is always unity. In Figure 5.3 and Figure 5.4 it is evident that damage evolves from zero to unity consistently. The damage evolution curves show that the damage rate increases with time and is critical at rupture, which is consistent with the physical phenomena of creep damage. In the KR model, the critical damage observed is between (0.2-0.3) suggesting that rupture takes place when damage is well below unity. This contradicts the continuum damage mechanics (CDM) theory upon which the KR model is based. This discrepancy of KR model is clearly shown in Figure. In this figure for both the KR and sinh model are able to model the creep strain to rupture; however the KR fails to accumulate damage to unity.

Figure 5.8 shows the creep rupture time prediction curves of KR and Sinh model in comparison to 304 SS data at 593°C, 843°C and 954°C respectively [66],[**67**]. The eq. (4.10) and (4.31) are

used to predict creep rupture life for the KR and Sinh models respectively. Figure 5.8(a) shows that the Sinh model better fits the experimental data collected from literature [66],[**67**]. The quality fit of the KR model gradually reduces from the low stress to high stress region. The KR rupture time prediction (on a log scale) changes linearly from the low stress to high stress region. As rupture time approaches zero the corresponding applied stress becomes astronomically higher than the ultimate tensile stress. Sinh model has the necessary bend in the model curve to better fit the experimental data in the high stress region. This problem can be further clarified by focusing on the high stress region as shown in Figure 5.8 (b). It shows that the Sinh curve meets the Y-axis around the ultimate tensile stress (UTS), 560 MPa (is consistent with physical phenomena of ductile failure) while the KR model keeps moving linearly upward from low stress to high stress and touches the Y-axis around 840 MPa an astronomical unrealistic value. In the sinh curve, the necessary bend takes place close to the yield stress (YS) of 304 SS[Figure 5.8(b)]. In Sinh model [Eq. 25] the constant σ_t performs as the bend initiator, where the curve bends when equivalent stress becomes equal to transition stress σ_t. It is well known that UTS and YS are functions of temperature. Accordingly the transition stress constant is also a function of temperature $\sigma_t = f(T)$, [Figure 5.8, Table 5.2]. KR model fails to do this necessary bent. Penny [**50**], described this ill-nature of the KR rupture model as the brittle curve phenomena and modified the KR model to accommodate the required (lowstress-highstress) bend by introducing additional factors and material constants while restraining the assumptions that critical damage is not unity; a violation of CDM. Gorash [**75**] proposed different types of creep behavior for high and low level stress, power law creep is for high stress region and viscous type creep for low stress region and formulated two different equations based on KR model to accommodate the required bend in the model curve, yet the characteristic damage is low (0.2-0.4) same as the KR model and becomes excessively high at about 90% of lifetime. The Sinh model accommodates the lowstress-high stress bend using only one equation and less material constants.

Chapter 6: Finite Element Simulation

6.1 Limitations of Kachanov-Rabotnov model in FEM analysis

Damage Localization

Localized damage prediction suggests that damage has occurred only on the cracked surface while the surrounding area of the component is still unaffected, which is unrealistic. This type of faulty prediction takes place if any damage variable of the prediction model presumes very localized homogeneity for damage distribution. The prediction model becomes unable to maintain the required elliptical nature, may lead to premature, perfectly brittle damage evolution response [77]. Liu & Murakami [64] has observed damage localization problem in homogeneous stress field even at very small (10^{-8}) stress gradient numerical error. Damage localization may be observed at very fine meshing. FEM analysis of KR model on thin circular notched (3 mm dia.) specimen with initial crack exhibits damage localization [Figure 6.1]. It is observed that damage ranged (0.22-.99) is locally distributed within 0.1 mm distance from the crack path (mesh size 0.05 mm). Upon further mesh refinement critically localized damage may be observed. In discussion sections this problem in discussed in detail.

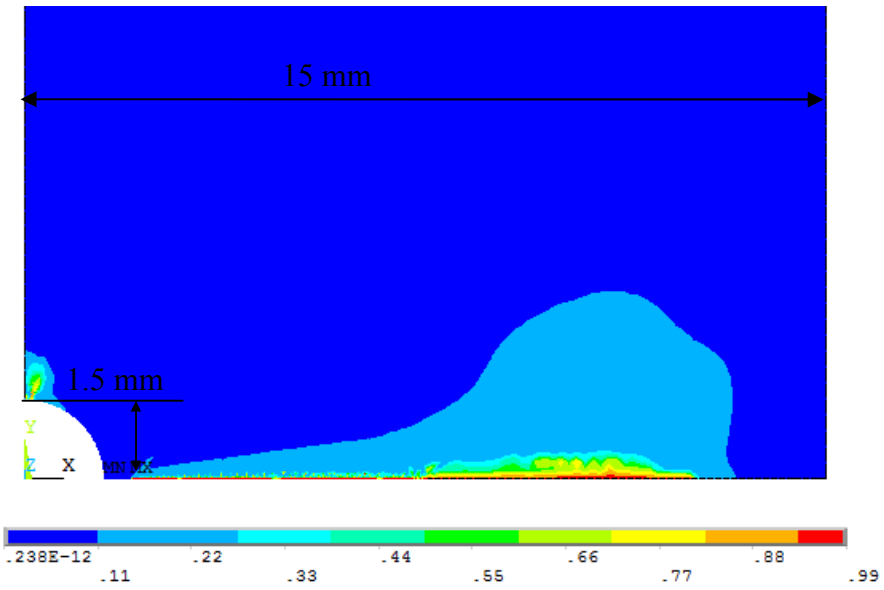

Figure 6.1: Typical KR damage localization

Mesh Dependency and Stress Singularity

All materials include some form of defects or voids. FEM analysis of notched specimen with initial crack are very popular and can emulate these phenomena. But sharp edge at initial crack tip can lead stress singularity. Refining mesh size will develop very high unrealistic stress values. Stress singularity can also be observed if the governing equation is stress sensitive as discussed in the stress sensitivity section. Peerling et al. [**76**] has explained this phenomena; as mesh is super-refined the fracture energy becomes zero and crack growth becomes infinite and originates mesh dependency.

6.2 NUMERICAL METHODOLOGY

For KR model [Eq. (4.5) & (4.6)] are used. And for Sinh model [Eq. 4.28, 4.29] are used. For both model stress is assumed as Hayhurst (triaxial) stress, redefined after each time step. It is defined as

$$\sigma_{HR} = \alpha\sigma_1 + 3\beta\sigma_m + (1-\alpha-\beta)\bar{\sigma} \tag{6.1}$$

where, σ_1 is the principal stress, σ_m is the hydrostatic mean stress, and $\bar{\sigma}$ is the net stress [**78**]. $\alpha \& \beta$ are the weighing factors ranging from zero to unity. The formulation is implemented into academic ANSYS FEM software. The user material routine (USERMAT) of ANSYS user-programmable feature (UPF) is used to define the KR and Sinh model constitutive behavior of material. Finally ANSYS Mechanical Parametric Design Language (APDL) tool is used to run the FEM analysis. ANSYS calls USERMAT for each Newton-Raphson iteration. ANSYS input stress, strain and all state variables at the beginning of each time increment iteration step. All values and tensors are stored in vector or matrix form makes easy to recall when needed [**79**].

Material constants of 304 SS at defined stress level and temperature are determined for KR and Sinh model. Process of finding the constants and their accuracy are discussed in the previous work of these authors [**74**]. KR and Sinh model uses different assumptions and concepts, thus material constant are different. Table 6.1 and 6.2 shows the constant for each model.

Table 6.1: KR model constant

	A ($MPa^{-n}\ hr^{-1}$)	n	M ($MPa^{-\chi}\ hr^{-1}$)	ϕ	χ
KR	6.53e-31	12.78	1.02e-10	12	3

Table 6.2: Sinh model constant

	A ($\%hr^{-1}$)	λ	M (hr^{-1})	ϕ	σ_s (MPa)	σ_t (MPa)
Sinh	1.28e-4	4.52	3.2e-2	5.4	29	289.8

The iteration starts with initial damage value $\omega(t) = 0.0$, and material element is assumed failed at $\omega(t) = 0.99$. The damage is restricted at 0.99 as failure instead of unity to avoid singularity may cause by $\omega(t) = 1.0$. The USERMAT is first used on a single three dimensional eight node elements with proper initial boundary conditions. The ANSYS results were compared with experimental data to check the accuracy of the USERMAT coding and to remove any miscoding that may lead to trivial solution.

6.2.1 Single 3D element (304 SS)

A uniform load of 160 MPa was applied on the top surface of the element. Material constants from Table are used. The simulation is run up to the experimental rupture time (167 hr) to facilitate comparison with experimental data. Histories of creep deformation (ε) and damage evolution (ω) of FEM analysis are saved in a data file and compared with experimental data, collected form literature [**65**]. Figure shows the comparison of ANSYS results of sinh and KR model with experimental data points. From the figure it is evident that the FEM curve goes through the scatter band of the experimental data. Both Sinh and KR model analysis fits the strain deformation, but corresponding damage is well below unity for KR model. Analytical damage data points of KR model does not reach to unity (One of the limitation of KR model) and the fitting simulation curve cannot rise to unity. Analytical damage of Sinh model at failure is unity. FEM simulation of Sinh model reaches unity at rupture accurately fitting the data points.

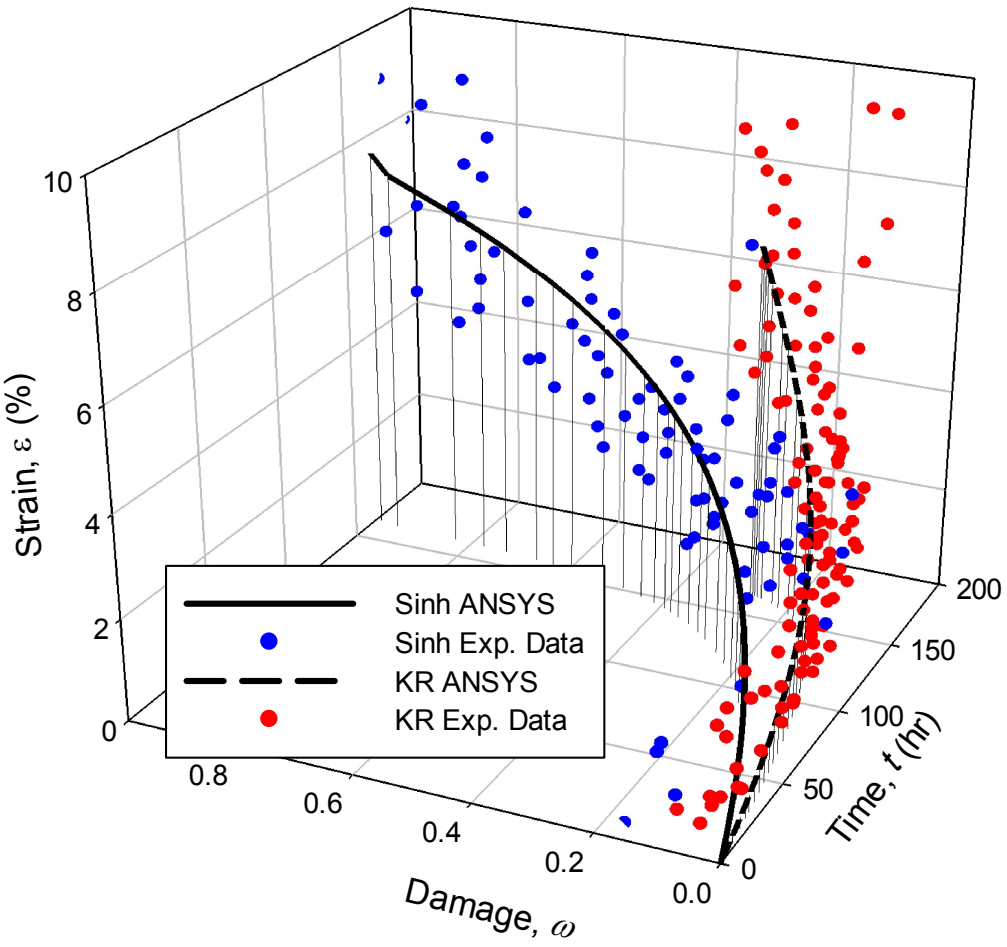

Figure 6.2: Comparison of sinh and KR FEM model

6.2.2 304 SS thin plate with circular hole

A uniform normal load is applied on the edge of the plate. Only one fourth of the symmetric specimen is modeled in finite element calculation. In order to observe mesh dependency (1/8 mm, 1/20 mm, 1/100 mm) were employed. Information of the finite element meshes are given in Table .3. A typical finite element meshing is shown in figure 6.5.

Table 6.3: Information about finite element meshes

Mesh	Size of element $\Delta e(mm)$	Number of elements	Number of nodes
1/8	0.125	3637	11172
1/20	0.05	4882	15013
1/100	0.01	19629	59882

Stress concentration at the crack tip changes with the changing mesh size for same applied load. Two different approaches are adopted to study this behavior named Fixed remote load approach and Adjusted crack tip load approach. In the first approach, remote applied load on the edge on the plate is kept constant, load concentration at the crack tip varied freely with the changing mesh size. A load of 100 MPa is applied on the edge of the plate with stress concentration factor $K_t = 3.0$. Stress at the crack tip is different for each mesh arrangement. In second approach, remotely applied load is changed to have exact same (552.52MPa) first time step stress at the crack tip. The remote applied load is different and the stress at the crack tip is same for all mesh arrangements.

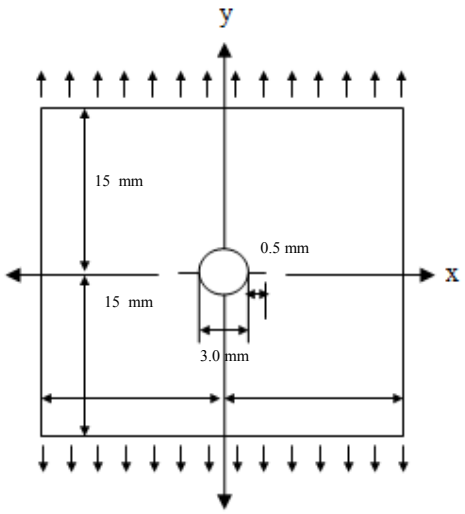

Figure 6.4: Thin 304 SS plate with circular hole

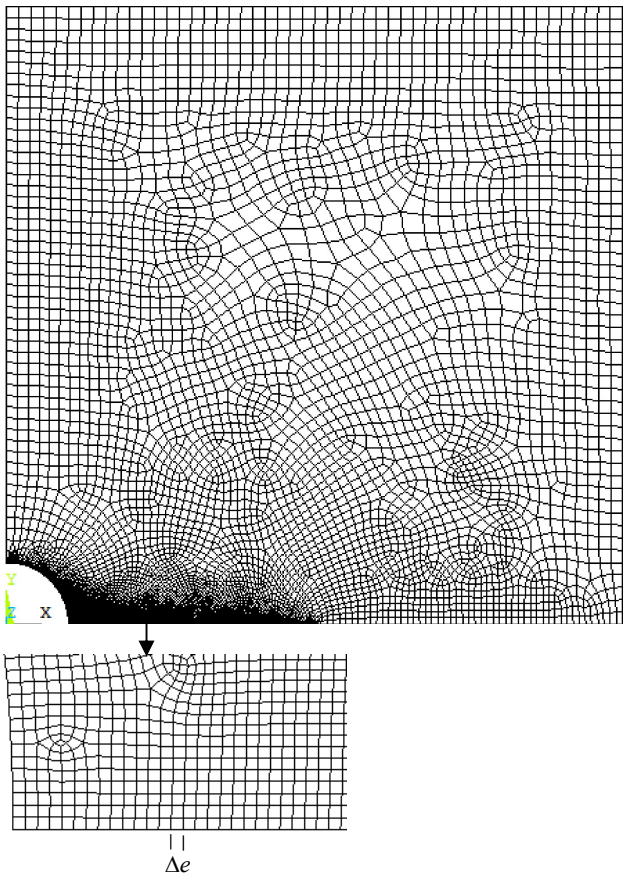

Figure 6.5: ANSYS FEM mesh (0.01 mm)

The USERMAT takes inputs from the command file(input deck) and begins iteration using provided constants. When damage starts to grow, the Young's modulus is redefined every time step by a simple equation as follows

$$young = young * (1 - \omega(t)) \tag{6.2}$$

The stress is defined in tensor form, new equivalent stress is defined after each time step using corresponding damage model by Newton-Raphson Iteration. Creep deformation and damage model rate is calculated, and builds up with increasing time steps. Elements are defined as totally damaged when accumulated damage is equal to 0.99 for that element. Required information are stored in state variables and recalled in the post-processing section. All contour plots have same zoomed in view, and scales are dawn using MATLAB software [**80**].

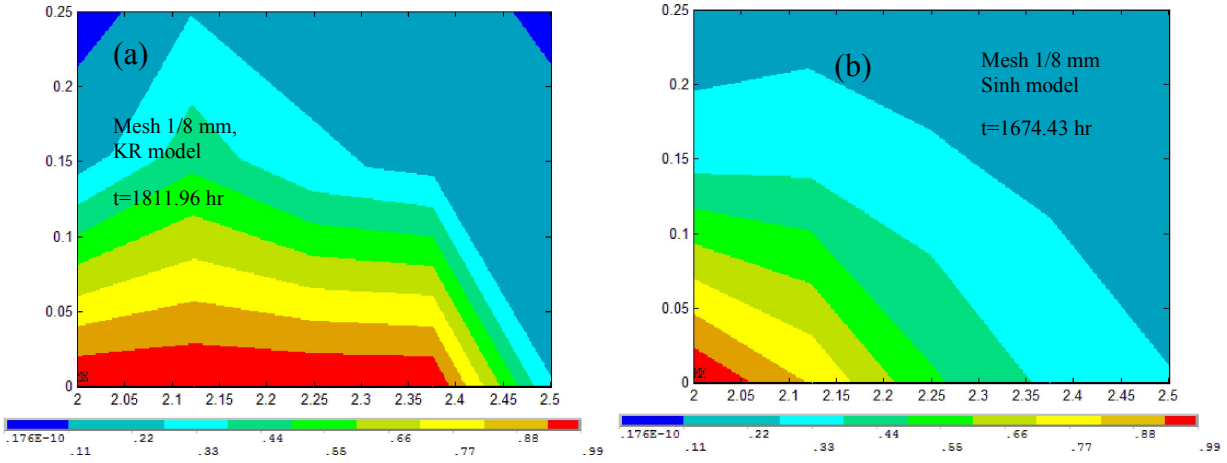

Figure 6.6: Damage distribution around the crack tip

6.3 FEM RESULT DISCUSSION

From figure 6.6 it is evident that Sinh model exhibits better distribution than the KR model (1/8 mesh). For sinh model when critical damage $(\omega = 0.99)$ is at 2.05 mm, the partial damage is distributed beyond 2.5 mm. Suggesting crack propagation is affecting the material matrix in front of the crack tip. Damage builds up gradually before cracked. For KR model damage ranging (0.88-0.33) is distributed in the vicinity of 2.4- 2.5 mm in front of the crack tip. KR model has 77% less distribution than Sinh model. Suggesting that damage is narrowly distributed only around the cracked surface and material is highly brittle. This behavior is the same as the problem shown in the figure 6.6. Sinh model shows more realistic damage distribution in front of the crack tip. This advantage of sinh model is also visible in vertical direction. Above the crack tip, the sinh model damage is more distributed than KR model.

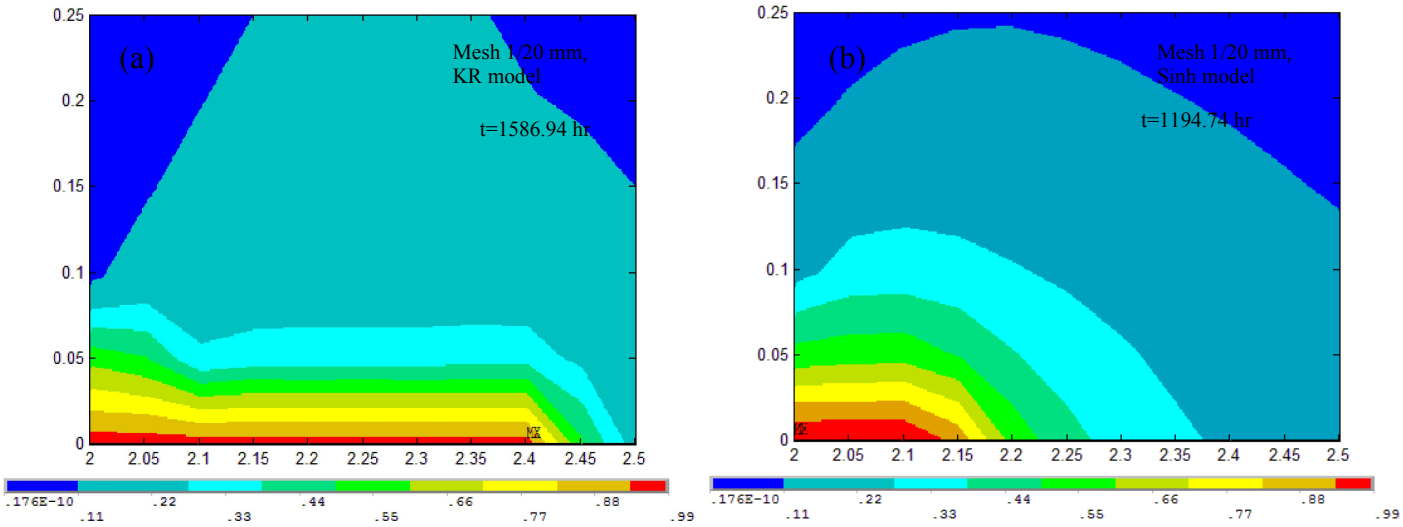

Figure 6.7: Damage distribution around the crack tip for (1/20 mm) mesh

In Figure 6.7, the same advantage of sinh model over KR model is observed. For finer mesh size (1/20 mm), the KR damage model becomes more localized and sinh model showing more realistic damage distribution around the crack tip. For sinh model damage ranging (0.88-0.33) is distributed over (2.14-2.37 mm) distance Figure 6.7 (a). For KR model damage ranging (0.88-0.33) is distributed over (2.41-2.49 mm) distance. KR model shows 65% less distribution than Sinh model. Sinh model has better distributed above and in front of the crack tip, while KR model is suggesting high localized unrealistic brittle damage.

In comparison of Figure 6.6 and Figure 6.7 it is evident that due to mesh refinement, KR model exhibits more mesh size and shape dependency than Sinh model. Due to mesh size change from 0.125 mm to 0.05 mm, KR damage distribution area drops almost to half. Sinh model has less damage distribution area drop than KR model, thus less mesh dependent. This phenomena is more visible upon further mesh refinement.

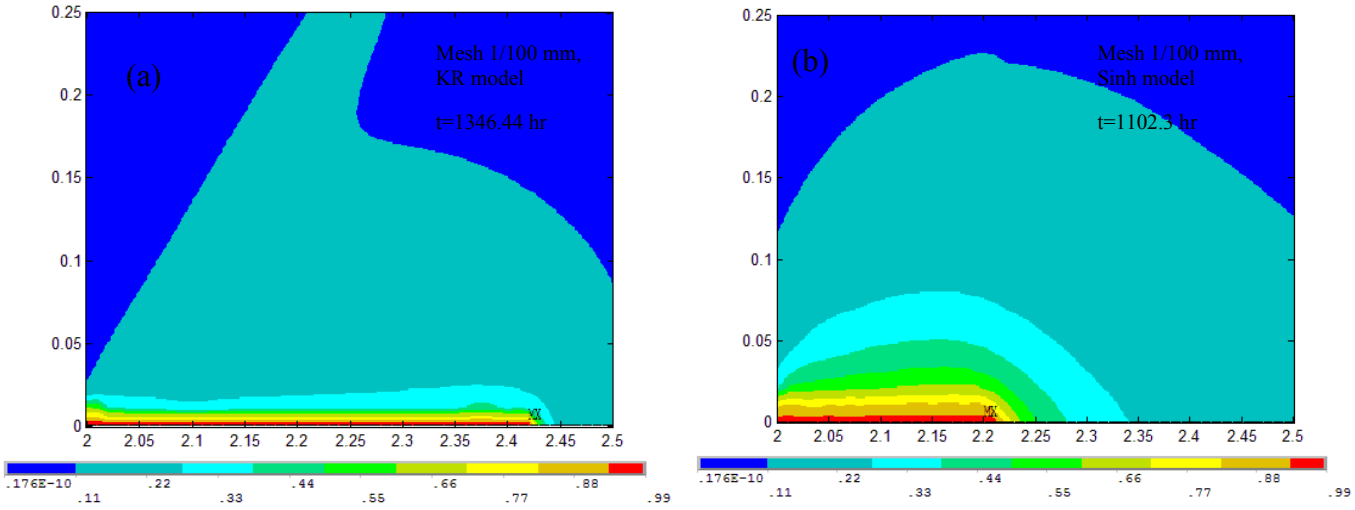

Figure 6.8: Damage distribution around the crack tip for (1/100 mm) mesh

Figure 6.8 shows the comparison of damage distribution between KR and Sinh model at 0.01 mm mesh size. The models behavior is same as discussed for Figure 6.6 and Figure 6.7. Sinh model has better damage distribution above and around the crack tip. The mesh refinement from 0.05 mm to 0.01 mm makes the KR damage further localized. In Figure 6.8 (a) most of damage distribution (0.88-0.33) above the crack is confined to below 0.05 mm and in front of crack tip, damage (0.88 -0.33) is confined over (2.42-2.44 mm) distance. In Figure 6.8 (b) Sinh model damage distribution (0.88-0.33) above the crack has better distribution. In front of the crack tip, damage (0.88-0.33) is well distributed over (2.22-2.34) mm distance. KR model shows 83% less damage distribution than Sinh model. Same phenomena are observed for adjusted crack tip load approach (second approach). For space limitation those figure are not included here.

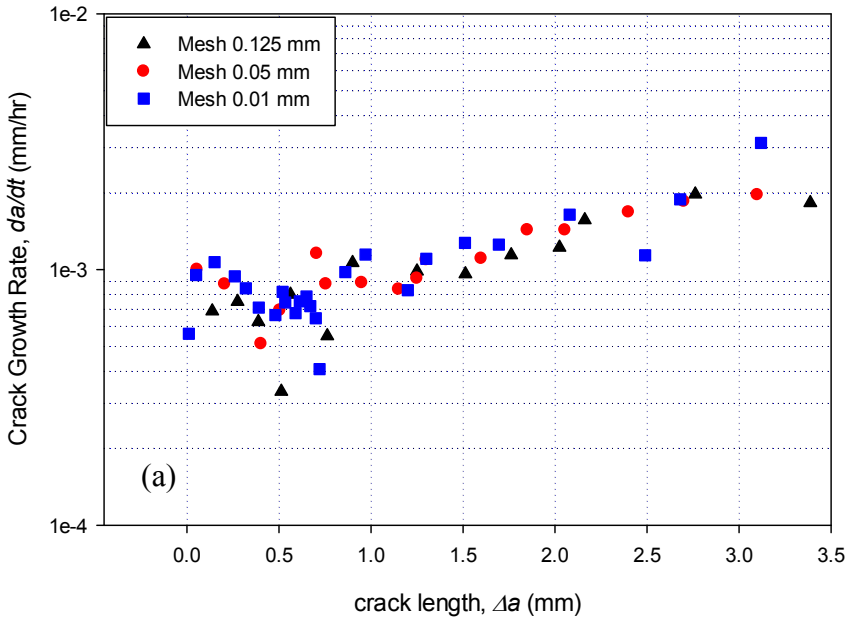

a) KR damage model crack growth rate

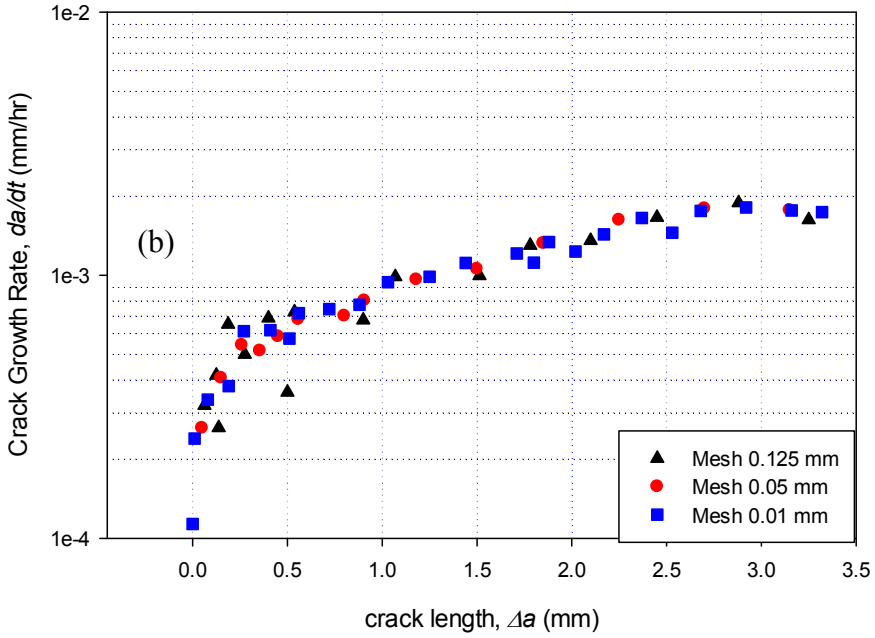

b) Sinh damage model crack growth rate

Figure 6.9: Mesh size effect on crack growth rate (Fixed remote load approach)

From figure 6.9 it is evident that for fixed remote load approach, Sinh model has less scatter than KR model. Upon mesh refinement KR model crack growth rate exhibits unstable behavior and more scattered. For KR model mesh refinement from 0.125 to 0.01 mm, gives increasing unstable wide scatter band of crack growth rate, suggesting that stress singularity may taking place at nodes. Load concentration at the crack tip is fluctuating with growing crack. Instead of gradually fall of the concentrated load of the propagating crack tip, it is observed by analyzing the FEM simulation state variable that for KR model, the load concentration does fluctuates. This fluctuation may causing the wide scatter band of the crack growth rate in Figure 6.9(a). From Figure 6.9 (b) shows that for sinh model crack growth rate is less affected with the mesh refinement. For all three mesh size the crack growth rate is almost the same and less scatter is observed. Figure 6.10 shows the crack growth rate dependency on mesh size when first time-step load at the crack tip is same (552.52 MPa) for all mesh size. Applied remote stress is adjusted for different mesh size to obtain same initial concentrated stress at the crack tip. The finer the mesh size, the lower the remote stress is required to get same load concentration at the initial crack tip. Form this figure; it is evident that for different mesh size KR model is more sensitive. KR model has higher crack growth rate compared to Sinh model crack growth rate for each mesh size. More scatter band is visible for KR model; Sinh model crack growth rate is almost uniform. For mesh size of 0.125 mm, KR model stopped running in FEM simulation after accumulated crack growth reached 2.0 mm. Stress singularities may take place to cause that problem. Larger element size is giving unrealistic values, and crack growth rate may become infinite. KR model is mesh dependent. For sinh model the crack growth rate is comparatively low, and simulation run far beyond crack growth 3.5 mm for all three mesh size. Sinh model exhibits comparatively less mesh dependency.

(a)

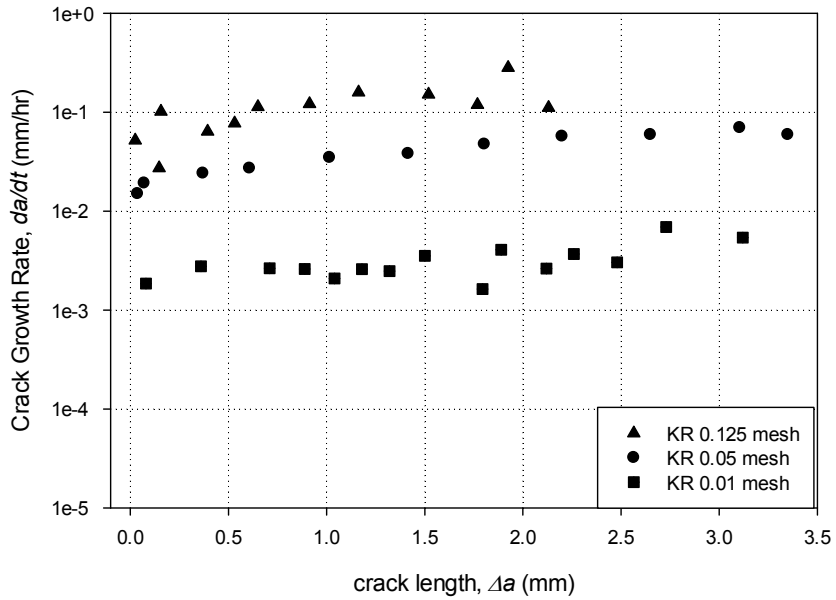

a) KR damage model crack growth rate

(b)

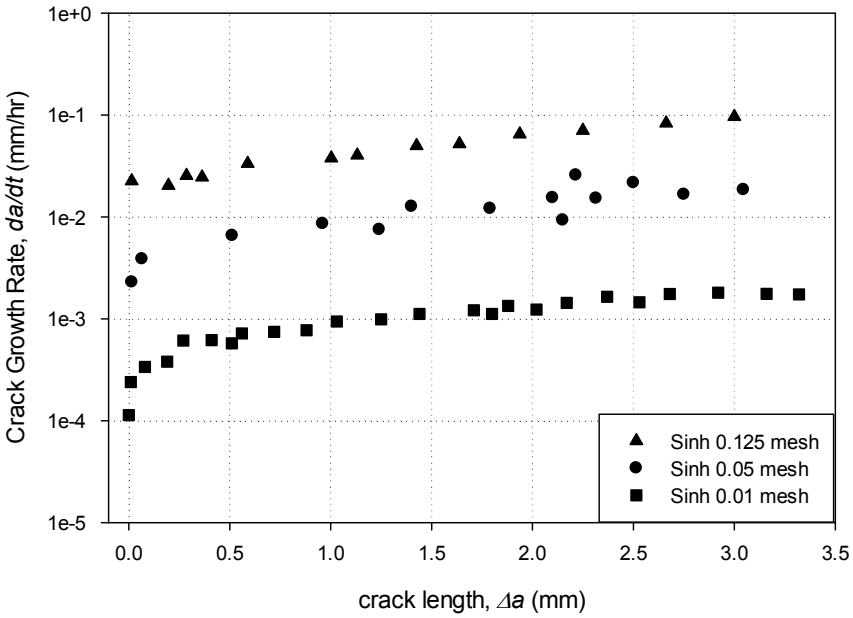

b) Sinh damage model crack growth rate

Figure 6.10: Mesh size effect on crack growth rate (Adjusted same crack tip load approach)

Chapter 7: Conclusion and Future work

7.1 CONCLUSION

The novel Sinh model has been found to produce a better prediction of the creep deformation of 304 SS than the KR model. The Sinh model is also easier to fit as it has one less constants. The constants are not dependent on each other like the KR model and the constants exhibit better temperature dependency when compared to the constants of the KR model. The Sinh model provides a consistent value for critical damage while the KR model does not. The analytical method for the Sinh model proves to be effective in finding the secondary and tertiary creep damage constants without extensive optimization. Parametric simulation, should be conducted over wide range of temperature and stress to validate the prediction capabilities of the sinh model under a multiaxial state of stress. Sinh model offers better creep damage and crack growth analysis. It is proved analytically and numerically that Sinh model is less sensitive to stress. It exhibits less damage localization than KR model in numerical analysis. In FEM analysis Sinh model exhibits less mesh dependency and less stress singularity compared to KR model. FEM analysis on 3D specimen can facilitate more real life phenomena study.

7.2 FUTURE WORK

This study establishes the Sinh model as a potential solution to the problems of some popular model. Further study will be conducted to analyze the capacity of this model.

Strain approach to the Sinh model

For future study strain approach to Sinh model will be studied. Introducing the damage equation to the strain rate equation gives a damage free equation. Upon integration it gives an erf (error) function. Assuming p=1 instead of p=2/3 for strain approach may solve this problem. Having two approaches to Sinh model will facilitate to quantify each approach by the other approach. Two approaches will provide better analysis of the model.

Notch strengthening study

FEM analysis of different size notch and multi notched specimen will facilitate the study the notch strengthening capacity of the Sinh model. FEM simulation of a 3D specimen will also be conducted. 3D specimen FEM simulation will facilitate more realistic study of this model. Constants will be defined as dependent variable of stress and temperature level. Experimental data sets at wide range of stress and temperature will be needed. Experiments will be conducted to define the Sinh model constants in the form of characteristic equation. The model simulation can be conducted for wide range of stress and temperature level.

Statistical study of Sinh model

No two experimental data are identical. Experimental data distribution are observed in literature. Statistical study will be conducted to produce a upper limit and the lower limit of the prediction. For a given operating condition (stress, temperature) the model will provide an experimental based predicted range with confidence value.

References

[1] Homji, C. B. M. and Gabriles, G. 1998. Gas Turbine Blade Failures-Causes, Avoidance, Aad Troubleshooting. 27th Turbomachinery Symposium. pp. 129.

[2] Wu, X. 2010. Life Prediction of Gas Turbine Materials. Gas Turbines. Gurrappa Injeti (Ed.). InTech.

[3] Bernstein, H. L. 1998. Materials issues for users of gas turbines. In Proceedings of the Twenty-Seventh Turbomachinery Symposium, Turbomachinery Laboratory, Texas A&M University, College Station, Texas (pp. 129-179).

[4] Manu, C. C. 2008. Finite Element Analysis of Stress Rupture in Pressure Vessels Exposed to Accidental Fire, MS Thesis, Queen's University, Kingston, Ontario, Canada.

[5] Stewart, C. M. 2013. A Hybrid Constitutive Model For Creep, Fatigue, And Creep-Fatuigue Damage. PhD Dissertation. University of Central Florida. Florida. USA.

[6] Dundas, R. E. 1982. The Use of Performance Monitoring to Prevent Compressor and Turbine Failures. ASME Gas Turbine Congress, Paper Number: 882-GT -66.

[7] Bloch, H. P. 1998. Improving machinery reliability (Vol. 1). Gulf Professional Publishing.

[8] Viswanathan, R., and Scheirer, S. T. 2001. Materials Technology for Advanced Land Based

Gas Turbines. Creep: proceedings of the international conference on creep and fatigue at

elevated temperatures, Tsukuba, Japan, No.01-201 (20010603), pp. 7-21.

[9] Hoeft, R., Janawitz, J., Keck, R. 2003. Heavy-Duty Fas Turbine Operating and Maintenance Considerations. GE Energy Services, GE Power Systems, Atlanta, GA.

[10] Meyers, M. A., & Chawla, K. K. 2009. Mechanical behavior of materials (Vol. 2, pp. 420-425). Cambridge: Cambridge university press.

[11] Lemaitre, J., Chaboche. 1985. J.L. Mechanics of Solid Materials. Paris: Cambridge University Press.

[12] Kraus, Harry. 1980. Creep Analysis. New York: John Wiley & Sons, 1980.

[13] Conway, J. B. (1969). Stress Rupture Parameters--Origin, Calculations And Use. Gordon And Breach Science Publishers, Inc., New York. 1969, 308 P.

[14] Penny, R. K., and Marriott, D. L., 1995, Design for Creep, Springer, pp.11

[15] B. Dyson, Use of CDM in Materials Modeling and Component Creep Life Prediction, Journal of Pressure Vessel Technology, August 2000, Vol. 122.

[16] F.T. Furillo, S. Purushothaman, Understanding the Larson-Miller parameter, Scripta Metallirgica, Vol.11, 1977.

[17] M. Vasudevan, S. Venkadesan, P.V. Sivaprasad, S.L. Mannan, Use of the Larson-Miller parameter to study the influence of ageing on the hardness of cold-worked austenitic stainless steel, Elsevier, pp. 251-255.

[18] R. J. Dimelfi, Understanding the Larson-Miller Parameter, Scripta Metallirgica, Vol. 12, pp. 327-329, 1978.

[19] Eureqa Desktop, Nutonian Inc., 212 Elm St. Suite 310, Somerville, MA 02144.

[20] S.S. Manson, A.M. Haferd, A Liner Time-Temperature Relation for Extrapolation of Creep and Strss-Rupture Data, National Advisory Committee for Aeronautics, Technical Notes 2890, March 1953.

[21] W. Bendick, L. Cipolla, J. Gabrel, J. Hald, New ECCC assessment of creep rupture strength for steel grade X10CrMoVNb9-1 (Grade 91), International Journal of Pressure Vessels and Piping, pp. 304-309 , 2010.

[22] D. J. Wilson, R. E. Marrone, J. W. Freeman, Larson-Miller and Manson-Haferd Parametric Extrapolation of Rupture Data for Type 304 (18Cr-8Ni), Grade 22 and Grade 11 Steel, Research Report, The University of Michigan, Ann Arbor, Michigan, 1968.

[23] D.R. Eno, G. A. Young, 2008. A Unified View of Engineering Creep Parameters, ASME Pressure Vessels and Piping Division Conference, July 21-31, Chicago, Illinois.

[24] Krempl, Erhard. 1979. An experimental study of room-temperature rate-sensitivity, creep and relaxation of AISI type 304 stainless steel. Journal of the Mechanics and Physics of Solids 27.5 (1979): 363-375.

[25] Keita, Oumar, Cristian Dascalu, and Bertrand François. "A two-scale model for dynamic damage evolution." Journal of the Mechanics and Physics of Solids 64 (2014): 170-183.

[26] Lindborg, U. "Creep cracks and the concept of damage." Journal of the Mechanics and Physics of Solids 16.5 (1968): 323-328.

[27] C. M. Stewart, and A. P. Gordon. 2010. Analytical Method to Determine the Tertiary Creep Damage Constants of the Kachanov-Rabotnov Constitutive Model. ASME, International Mechanical Engineering Congress and Exposition,177-184.

[28] C. M. Stewart, and A. P. Gordon.2011. Strain and Damage-Based Analytical Methods to Determine the Kachanov-RabotnovTertiary Creep Damage Constants. International Journal of Damage Mechanics, 21(8) (2011), 1186-1201.

[29] R. Larson, and J. Miller. 1952. A Time-Temperature Relationship for Rupture and Creep Stress. Transactions of the ASME, 74 (1952), 765.

[30] F. Monkman, and N. Grant, Proc. of ASTM, 56 (1956), 595.

[31] A. Cauvin, R. B. Testa. 1999. Damage mechanics: basic variables in continuum theories," International Journal of Solids and Structures, 36, 747-761.

[32] J.J. Marigo. 1985. Modeling of Brittle and Fatigue Damage for Elastic Material by Growth of Micro-voids. Engineering Fracture Mechanics, vol. 21, 861-874.

[33] Lindborg, U. 1968. Creep cracks and the concept of damage. Journal of the Mechanics and Physics of Solids 16.5, 323-328.

[34] Ibijola, E. A. 2002. On some fundamental concepts of continuum damage mechanics. Computer methods in applied mechanics and engineering 191.13 (2002): 1505-1520.

[35] Lemaitre, Jean. 1985. A continuous damage mechanics model for ductile fracture. Journal of Engineering Materials and Technology 107.1, 83-89.

[36] J.L. Chaboche. 1978. Description thermodynamique et phenomenologique de la visco-plasticite cyclique avec endommagement, Theses Dissertation, University of Paris 6.

[37] J.P. Cordebois, F. Sideroff. 1982. Endommagement anisotrope delasticite et plasticite, Journal Mech. Theor. Appl. Special issue.

[38] Raghavan, P., and S. Ghosh. 2005. A continuum damage mechanics model for unidirectional composites undergoing interfacial debonding." Mechanics of materials 37.9. 955-979.

[39] Hill, R. 1963. Elastic properties of reinforced solids :some theoretical principles," Journal of Mechanics, Physics and Solids. 11, 357-372, 1963.

[40] Hashin, Z.," Analysis of composite materials," Journal of Applied Mechanics 50 , 481-505, 1983.

[41] Lemaitre, J., Chaboche, J-L, 1990, Mechanics of Solid Materials, Cambridge University press.

[42] Voyiadjis, G.Z., Kattan, P.I., "Advances in Damage Mechanics: Metals and Metal Matrix Composites.," Elsevier, 1999.

[43] M. Oyane, Criteria of Ductile fracture strain, Bull. JSME 15 (1972) 1507.

[44] G. Rousselier, Ductile fracture models and their potential in local approach of fracture, Nucl. Fngrg. Design105 (1987) 97-111.

[45] J. C. Simo, J.W. Ju, Strain and stress-based continuum damage models- I Formulation, Int. J. Solids Struct. 23 (7) (1987) 821-840.

[46] W. Qi, and A. Bertram, “Damage modeling of the single crystal superalloy SRR99 under monotonous creep,” Computational materials science, 13(1) (1998), 132-141.

[47] J. Lemaitre, A Course on Damage Mechanics (Berlin, Springer, 1992).

[48] J. L. Chaboche, 1981, "Continuous Damage Mechanics- A tool to describe phenomena before crack initiation," Nuclear engineering and design, 64.2 (1981), 233-247.

[49]R. K. Penny & M. A. Weber, Robust Methods of Life Assessment during Creep, Int. J. Ves. & Piping 50 (1992) 109-131.

[50] R K Penny, The use of damage concept in component life assessment, Int. J. Pres. Ves. & Piping 66 (1996) 263-280.

[51] S. Murakami, Y. Liu, and M. Mizuno, 2000, "Computational methods for creep fracture analysis by damage mechanics," Comput. Methods Appl. Mech. Engrg.,183 (2000), 15-33.

[52] Liu, Y., Murakami, S., Kanagawa, Y., 1994. Mesh-dependence and stress singularity in finite element analysis of creep crack growth by continuum damage mechanics approach. Eur. J. Mech. A/Solids 13, 395–417.

[53] Z. P. Bazant, and G. Cabot Pijaudie, "Nonlocal continuum damage, localization instability and convergence," J. Appl. Mech. Trans. ASME, 55 (1988), 287-294.

[54] Ladeveze, P. "A damage computational method for composite structures."Computers & Structures 44.1 (1992): 79-87.

[55] P. G. McVetty, "Creep of Metals at Elevated Tempeartures – Hyperbolic-Sine Relation Between Stress and Creep Rate" Transactions of the ASME, 65(7) (1943), 761-767.

[56] C. Phaniraj et al., "The Relationship between Transient and Steady State Creep in AISI 304 Stainless Steel," Acta Metallurgica et Materialia, 39(7) (1991), 1651-1656.

[57] J. F. Wen, S. T. Tu, et al, Simulations of creep crack growth in 316 stainless steel using a novel creep-damage model, Engineering Fracture Mechanics , 98 (2013) 169-184.

[58] C. J. Hyde, T.H. Hyde, et al, Damage mechanics based predictions of creep crack growth in 316 stainless steel, Engineering Fracture Mechanics 77 (2010) 2385-2402.

[59] P. G. McVetty, "Creep of Metals at Elevated Tempeartures – Hyperbolic-Sine Relation Between Stress and Creep Rate" Transactions of the ASME, 65(7) (1943), 761-767.

[60] M. Lawa, W. Payten, K. Snowden, Finite element analysis of creep using Theta projection data, International Journal of Pressure Vessels and Piping 75 (1998) 437–442.

[61] ASTM Standard A276, 2013, "Standard Specification for Stainless Steel Bars and Shapes," ASTM International, West Conshohocken, PA.

[62] D. J. Wilson, R. E. Marrone, J. W. Freeman, Larson-Miller and Manson-Haferd Parametric Extrapolation of Rupture Data for Type 304 (18Cr-8Ni), Grade 22 and Grade 11 Steel, Research Report, The University of Michigan, Ann Arbor, Michigan, 1968.

63] C. J. Hyde, T.H. Hyde, et al, Damage mechanics based predictions of creep crack growth in 316 stainless steel, Engineering Fracture Mechanics 77 (2010) 2385-2402.

64] Liu, Yan, and Sumio Murakami. "Damage Localization of Conventional Creep Damage Models and Proposition of a New Model for Creep Damage Analysis."JSME International Journal Series A 41.1 (1998): 57-65.

[65] Kim, Seon-Jin, et al. "Statistical properties of creep rupture data distribution for STS304 stainless steels." Materials Science and Engineering: A 483 (2008): 529-532.

[66] . Booker, M. K. Use of generalized regression models for the analysis of stress-rupture data. Oak Ridge National Lab., TN (USA), 1978.

[67] Bynum, J. E., Ellis, F. V., Roberts, B. W., and Canonico, D. A., 1992, "High Temperature Creep of Type 304 Stainless Steel," Stress Classification, Robust Methods, and Elevated Temperature Design; presented at the 1992 Pressure Vessels and Piping Conference, New Orleans, La, pp. 67-83.

[68] J. L. Chaboche, "Lifetime predictions and cumulative damage under high-temperature conditions," Low-Cycle Fatigue and Life Prediction, ASTM STP,770 (1982), 81-104.

[69] J. L. Chaboche, "Anisotropic creep damage in the framework of continuum damage mechanics," Nuclear Engineering and Design, 79(3) (1984), 309-319.

[70] J. J. Skrzypek, , and A. Ganczarski, Modeling of material damage and failure of structures: Theory and applications, (Berlin Heidelberg ,Springer-Verlag, 1999).

[71] C.M. Stewart, "Tertiary Creep Damage Modeling of a Transversely Isotropic Ni-based Superalloy," (MS thesis, University of Central Florida, Orlndo, Fl, 2008).

[72] L. M. Kachanov, The Theory of Creep, National Lending Library for Science and Technology, (Boston Spa, England, Chaps. IX, X, 1967).

[73] Y. N.Rabotnov, Creep Problems in Structural Members, (Amsterdam, Weinheim,North Holland, WILEY-VCH Verlag GmbH & Co. KGaA, 1969).

[74] M.S. Haque, C. M. Stewart, 2015," Comparison of a new Sinh-hyperbolic creep damage constitutive model with the classic Kachanov-Rabotnov model using theoretical and numerical analysis, TMS, 144th Annual Meeting and Exhibition, Florida, USA, March 15-19,2015.

[75] Gorash, Y, 2008, "Development of a creep-damage model or non-isothermal long-term strength analysis of high-temperature components operating in a wide stress range," Martin Luther University of Halle-Winttenberg, Halle Germany.

[76] Peerlings, R. H. J., et al., 2002, "Localization issues in local and nonlocal continuum approaches to fracture," European Journal of Mechanics-A/Solids 21.2, pp 175-189.

[77] Hayhurst, D. R., Dimmer, P. R., Morrison, C. J., 1984, "Development of continuum damage in the creep rupture of notched bars," Philosophical Transactions of the Royal Society of London. Series A, Mathematical and Physical Sciences 311.1516, 103-129, London.

[78] Stewart, C. M., & Gordon, A. P., 2009, "Modeling the Temperature Dependence of Tertiary Creep Damage of a Ni-Based Alloy", Journal of Pressure Vessel Technology, 131(5), 051406.

[79] ANSYS Academic Research, Release 15.0, Mechanical APDL, ANSYS, Inc.

[80] MATLAB 8.0 and Statistics Toolbox Release R2011a, The MathWorks, Inc., Natick, Massachusetts, United States.

[81] H. C. Furtado, I. L. May, et al, Extrapolation of shorter time creep rupture data using the damage mechanics approach of penny.

[82] L may, H. C. Furtado, Creep damage assessment and remaining life evaluation, International Journal of Fracture, 97: 125-135, 1999.

Vita

My name is Mohammad Shafinul Haque. I have earned my Bachelors degree in mechanical engineering (BSc in ME, 4 year degree) from Khulna University of Engineering and Technology (KUET), Khulna, Bangladesh. I have completed my degree requirement for Masters in mechanical engineering here at University of Texas El Paso (UTEP). This thesis is submitted as a requirement of the degree including my research works throughout my graduate level study under the supervision of Dr. Calvin M Stewart.

This presented work is been published/submitted in the following publications:

1) Haque, M. S., and Stewart, C. M. 2014. Creep Rupture Life Prediction of 304 STS Using Larson-Miller Approach. 4th Southwest Energy Science and Engineering Symposium. El Paso, Texas, April 21, 2014.

2) Haque, M. S., and Stewart, C. M., "Limitation of Classic Local Approach KachanovRabotnov Creep Damage Model," 5th Southwest Energy Science and Engineering Symposium" El Paso, Texas, April 4, 2015.

3) M. S. Haque, C. M. Stewart, "Comparison of a new Sinh-hhyperbolic creep damage constitutive model with the classic Kachanov-Rabotnov model using theoretical and numerical analysis", TMS, 144th Annual Meeting and Exhibition, Florida, USA, March 15-19, 2015.

4) M. S. Haque, C. M. Stewart. A Novel Sin-Hyperbolic Creep Damage Model to Overcome the Mesh Dependency of Classic Local Approach Kachanov-Rabotnov Model. International Mechanical Engineering Congress & Exposition. IMECE15. November 13-19, 2015, Houston, Texas, USA (submitted)

5) M. S. Haque, C. M. Stewart. Theoretical And Numerical Analysis Of A New Sin-Hyperbolic Creep Damage Constitutive Model. Journal of Mechanics Physics of Solids. (submitted)

Contact information:

Mohammad Shafinul Haque, email: *mhaque@miners.utep.edu*, cell: 915-731-3449

mailing address: 1127 Los Angeles Dr., Apt#7, El Paso, Texas, USA.

This thesis/dissertation was typed by Mohammad Shafinul Haque.